Report on IDAL Network Plus Feasibility Project:

Feasibility of a novel non-pneumatic wheelchair tyre with adaptive spoke technology

Authors

Lead Applicant:	Otis Wyatt, Staffordshire University.
Principal Investigator:	Panagiotis Chatzistergos, Staffordshire University.
Co-Investigators:	Nachiappan Chockalingam, Staffordshire University.
	Evangelia Ganniari-Papageorgiou, Warwick University.

Acknowledgements

This project was funded by the Engineering and Physical Sciences Research Council [grant number: EP/W00717/1] through TIDAL Network Plus - Transformative Innovation in the Delivery of Assisted Living Products and Services.

Support from the Staffordshire Advanced Manufacturing Prototyping and Innovation Demonstrator (SAMPID), (partially funded by the European Regional Development Fund, project reference No: 32R19P03142) and the Turing funding scheme is acknowledged.

What we set out to discover:

Background and research context

Research on assistive technology (AT) for mobility is mainly focused on powered wheelchairs, prosthetics/orthotics, functional electrical stimulation, and robotic exoskeletons (Cowan et al., 2012). There is relative scarcity of research involving manual wheelchairs, even though they are among the most commonly used AT devices. According to WHO, 1% of people worldwide require a wheelchair, and about 0.5% require prosthetics/orthotics (World, 2017)(WHO, 2008). This demonstrates that a larger population is being neglected by research as clear problems have been shown in the literature (including musculoskeletal injury due to overexertion, back pain, pressure sores (Mason et al., 2020)).

Comfortable, manoeuvrable wheelchairs with good wheeling efficiency are extremely important to prevent injury and improve the quality of life of wheelchair users. There are several factors which contribute to these properties, with the key contributing component being the tyres of the wheelchair (Mclaurin & Brubaker, 1991). Wheelchair users are faced with two options when choosing their tyres: solid or pneumatic (Rodrigo & Herrera, 2018). Whilst it has been proven in literature that pneumatic

tyres are generally superior in terms of comfort and wheeling efficiency (Rodrigo & Herrera, 2018)(Sawatzky et al., 2004), many wheelchair users choose solid tyres as they do not puncture, they are maintenance free, and are longer lasting. However, tyres with low wheeling efficiency (namely solid tyres) can cause overexertion, which can lead to shoulder, wrist, and hand pain/injuries (Flemmer & Flemmer, 2016). On the other hand, the suspension and wheeling properties of pneumatic tyres are directly tied to the inflation pressure, and this reduces over time which causes sub-optimal performance, and a puncture renders the tyre ineffective (Gent & Walter, 1977). Wheelchair users therefore have to make substantial sacrifices with either tyre technology, and so new technology is required to overcome this problem.

Engineering / research challenge and why it matters

Optimising user comfort, and wheelchair manoeuvrability and wheeling efficiency on an individual basis is an extremely challenging process with current tyre technology. Implementing a new Flexible Spoke Non-Pneumatic Tyre (FS-NPT) technology in existing wheelchairs can help address this challenge. This technology is based on flexible spoke designs with tuneable mechanical behaviour, and it has never been used in wheelchairs before. Whilst the term 'spoke' is often used for the metallic/composite struts which connect from a typical wheelchair wheels' central hub to the outer wheel rim, it is also commonly used in literature to describe the plate configurations that make up the design of a non-pneumatic tyre, for example, a honeycomb spoke design. In this study, the terms 'spoke', or 'flexible spoke' will refer to the spokes of a non-pneumatic tyre. Previous work has involved elements of co-creation with wheelchair users to assess their needs regarding their tyres and building on the findings, it was discovered that FS-NPTs can replicate the mechanical characteristics of pneumatic tyres whilst being more lightweight (Wyatt et al., 2021). Spoke designs from literature were used and the feasibility of wheelchair FS-NPTs was tested for simple static loading conditions. Validating their capacity for optimum performance during different tasks of daily living is necessary to achieve a meaningful change in wheelchair technology. Spoke designs that are distinctively different to what has been previously used are needed to this end.

Aims and objectives for the project

This study aims to test whether it is feasible to significantly enhance the performance of manual wheelchairs by replacing existing wheelchair tyres with a novel FS-NPT technology. This will be achieved by designing, manufacturing, and assessing unique FS-NPT structures with capabilities that can enhance performance and are impossible using existing tyre technologies. To this end, our specific objectives are:

1. To develop a novel FS-NPT design that adapts its stiffness for different loading scenarios.
2. To demonstrate the feasibility of user-specific tuning and optimisation of tyre properties.

Adaptability to different loading scenarios will include becoming softer under impact loading for better cushioning during curb dismount, becoming stiffer during propulsion to improve wheeling efficiency, and softer during braking to help with direction changes. The ability for user-specific tuning

will enable optimising tyre performance according to a person's characteristics (e.g. body mass) and needs (e.g. level of activity, environment).

Flexible spoke non-pneumatic tyres

This section provides background knowledge of FS-NPTs. Figure 1 shows a diagram of an FS-NPT with honeycomb structure.

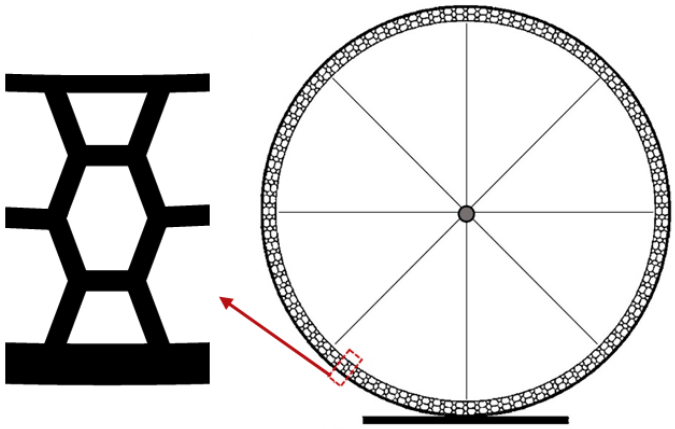

Figure 1 - FS-NPT diagram showing the whole tyre and a zoomed section of a single spoke with honeycomb design.

FS-NPTs consist of multiple deformable hyper-elastic spokes (usually of polymeric material) that replicate the behaviour of the internal air pressure in pneumatic tyres. A typical FS-NPT structure comprises flexible spokes, an external rubber tread, and an outer-ring that is sandwiched between the spokes and the tread (Zmuda et al., 2019). The outer-ring maintains the structural integrity of the tyre and has a very low thickness, and the tread is responsible for providing grip/traction. These tyres can have varied structured spokes which can influence the performance of the tyre.

The vertical (or radial) stiffness of a tyre is quantified as the vertical force applied divided by the resultant vertical displacement (kN/m). According to literature, the vertical stiffness in general determines the driver comfort (Dudziak et al., 2020). A tyre with lower vertical stiffness will have higher suspension properties than a more rigid tyre, leading to increased dampening of shocks and vibrations to provide a more comfortable wheelchair (Sawatzky et al., 2004). An FS-NPT can hypothetically improve comport further by adapting its vertical stiffness to a particular load. For example, buckling of the spokes (non-linear/large displacement behaviour) causes the stiffnesses of the spokes to change, and this buckling threshold can be tuned to occur at different loads. Buckling however should not occur under the weight of the user. The ground reaction force as a result of the tyre dropping from a particular height is also linked to user comfort, where lower reaction forces result in less force transmitted to the user and thus higher comfort is achieved (Dorfi, 2004). Therefore, a comfortable tyre is likely to demonstrate low peak ground reaction forces during impacts (comfortable footwear has shown to exhibit low ground reaction forces which could be applicable here (Dinato et al., 2015).

According to literature, the rotational stiffness of a tyre determines the efficiency of propulsion and also influences the tyre's rolling resistance (Deng et al., 2023). A tyre with high rotational stiffness will have lower energy losses caused by circumferential deformation of the tyre and will be easier for a user to propel. A low rotational stiffness can also be useful for aiding with braking, and it is hypothesised that some asymmetric FS-NPT designs may be capable of achieving different rotational stiffnesses simultaneously.

In the next section, single spoke models are used to represent the behaviour of an entire FS-NPT. As these spokes are not interconnected, their behaviour can be predicted in this way whilst significantly reducing software computational time. This also enables manufacturing of the spokes individually, creating a modular design which is beneficial for longevity and is sustainable.

What we did

This section is categorised into three main parts. These are the experimental testing of wheelchair tyre technology, the numerical testing of single spoke models, and the development of an FS-NPT prototype.

Testing of wheelchair tyre technology to obtain baseline mechanical behaviour

A tyre testing rig was developed (Figure 2) to assess the mechanical behaviour of current wheelchair tyre technology and to ultimately assess the first wheelchair FS-NPT (testing rig concept in Appendix 1). An aluminium beam was attached to a hinge to allow the beam to freely rotate. At the end of this beam, small aluminium extrusions were assembled in a configuration that resembles the 'fork' structure on a bicycle that attaches to the wheel, which holds the wheel rigidly on both sides. A steel shaft was inserted through the wheel and fork, connecting the wheel to the testing rig, and allowed a place for weights to be applied. The wheel was connected via bearings and nuts to enable rotation with high stability. Counterweights were used to counterbalance the structure to ensure that only the force from the weight of the wheel was acting on the force plate which the tyre was positioned directly over. The hinge was elevated via boxes to ensure that the aluminium beam was parallel with the floor.

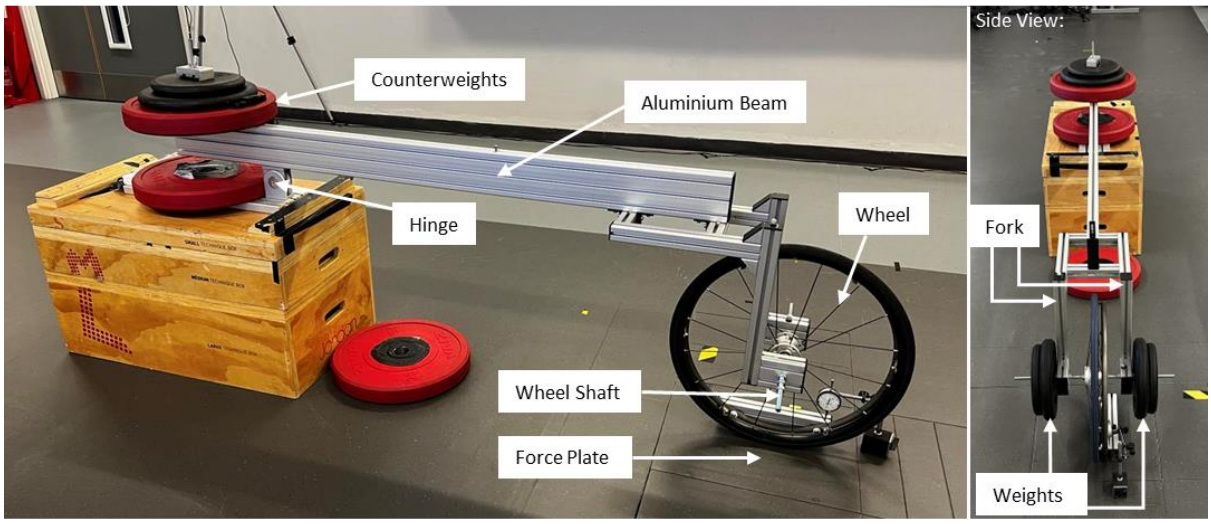

Figure 2 - Wheelchair tyre testing rig assembly. A hinge and beam structure enabled only vertical translation at the wheel side of the beam. A fork-like structure created from aluminium extrusions allowed attachment of a wheelchair wheel

(positioned atop the force plate). A steel bar acts as the wheel shaft which enabled the application of weighed plates. Counterweights negated the weight of the rig.

To obtain baseline data of current tyre technology, six different wheelchair tyres were selected for testing. These consisted of two solid tyres and four pneumatic tyres with varied mass, tread patterns, and recommended inflation pressures. These tyres all had the same inner diameter to allow them to fit onto a 24" Fusion 16 spoke wheel. The tyres specifications are shown in Table 1 and they are presented visually in Figure 3 along with their mass. All components were weighed using standard digital scales with a 0.001kg resolution. Scales were zeroed between measurements. In the setup for testing, the pneumatic tyres were inflated to the manufacturers' recommended inflation pressure, which was 758 kPa for all tyres except for pneumatic tyre 2 (Cheng Shin, grey) which was inflated to 448 kPa (Table 1).

Table 1 - Wheelchair tyre specifications.

Tyre Type (Abbreviation)	Make / Model / Sizes	Description
Solid Tyre 1 (S1)	Greentyre – 24 x 1	Smooth Tread / Curved Internal
Solid Tyre 2 (S2)	Greentyre – 24 x 1 (20 x 22 rim)	Flat Internal (alternate to S1)
Pneumatic Tyre 1 (P1)	Primo (V-Trak) C1025 – 24 x 1 (25-540)	Light blue tyre inflated to 758 kPa
Pneumatic Tyre 2 (P2)	Cheng Shin (IA2803) – 24 x 1.3/8 (37-540)	Grey tyre inflated to 448 kPa
Pneumatic Tyre 3 (P3)	Schwalbe Marathon Plus – 24 x 1 (25-540)	Black tyre inflated to 758 kPa
Pneumatic Tyre 4 (P4)	Kenda (23-540)	Navy blue tyre inflated to 758 kPa

Figure 3 - Images of wheelchair tyres (S=Solid, P=Pneumatic), pneumatic tyre inner tube, and Fusion 16 spoke wheel used for testing. Mass is also shown in grams.

Vertical stiffness was measured by incrementally increasing loading on the wheel shaft using calibrated weights to produce reaction forces equal to the average weight of a wheelchair user over one-wheel (Figure 4) (Sonenblum et al., 2016). Weights were applied in increments of 10kg up to a maximum of 30kg. For each increment of loading, the vertical deformation of the tyre was measured

using an extensometer (LINEAR, 0.01mm resolution) which was positioned on a handrail-attached beam that was checked to be parallel to the floor using a spirit level. The vertical reaction force resulting from the applied load was recorded by the force plate beneath the tyre (AMTI OPT464508HF AMTI, USA; sampling rate 1200Hz). All measurements were taken one minute after loading to account for any viscoelastic effects. Equivalent vertical stiffness was measured by dividing maximum reaction force by maximum displacement. Tests were repeated three times for each tyre.

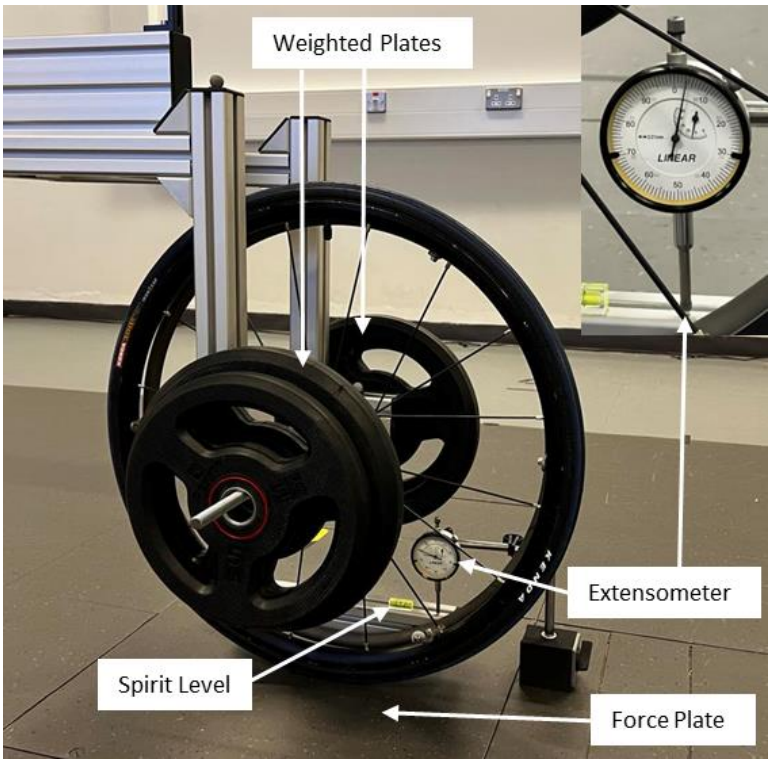

Figure 4 - Tyre testing rig setup for vertical loading. Weighted plates positioned on the steel axle applied a vertical load. An extensometer positioned on the handrail beam measured tyre displacement. The force plate recorded ground reaction forces.

Rotational stiffness was measured by first applying a vertical load simulating the weight of an average wheelchair user (over one wheel) before incrementally increasing the rotational moment on the beam attached to the wheel's handrail using suspended weights (Figure 5). The applied moment was increased to a maximum value of 25Nm by changing the distance of the suspended weights from the tyre's central hub (increments of 5Nm). The maximum applied moment corresponds to average values from literature for a user's initial wheeling stroke on a level surface (Koontz et al., 2005). The actual rotational moment applied to the wheel was calculated as the product of the generated parallel to the ground reaction force (measured by the force plate) and the distance between the tyre hub and the ground. A digital goniometer (Neoteck Level Box, 0.01° resolution) positioned at the end of the beam closest to the tyre (to avoid measuring any beam deflection) was used to measure the rotational deformation of the tyre (in degrees) for each increment of moment. The goniometer was reset after loading and unloading of each incremental weight to allow assessment of all results independently (results not tied to specific test number), and measurements were taken after unloading to measure tyre slippage. All measurements were taken one minute after loading to account for any viscoelastic effects. Equivalent rotational stiffness was calculated by dividing maximum applied moment over the

resulting rotation. All tests were repeated three times for each tyre to ensure there was minimal variability.

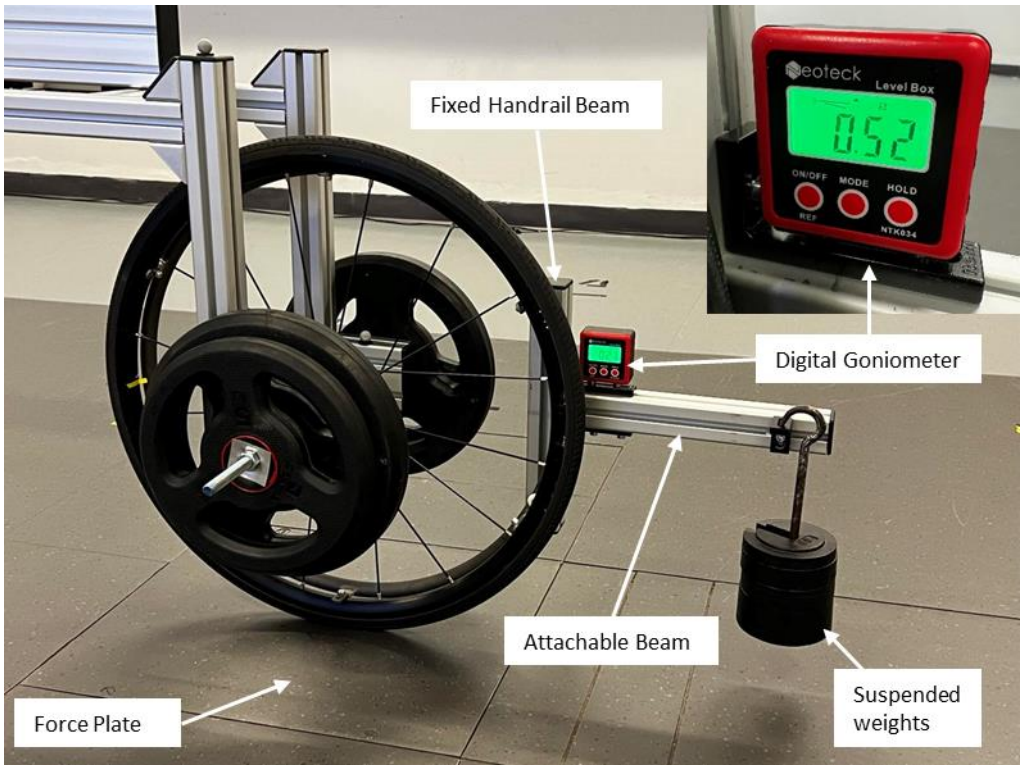

Figure 5 - Tyre testing rig setup for rotational loading (the maximum load from the vertical loading test was applied). Weights suspended on a second beam applied a rotational moment. A digital goniometer placed on the beam measured tyre rotational displacement. The force plate recorded ground reaction forces.

Impact reaction force was measured by, like before, applying a vertical load simulating the weight of an average wheelchair user (over one wheel). The attachable beam was removed, and a mechanical lifting hoist was connected to the end of the large aluminium beam via a ratchet strap and cable ties (Figure 6). The apparatus was lifted to create a gap of 5cm between the ground and the lower exterior of the tyre. A 5cm gap value was obtained from literature to simulate pavement/kerb dismounts (Initiative, 2019)(ISO, 2014). Cameras and markers (Vicon Vantage V5 optical cameras 240fps, Vicon retroreflective markers) were used to determine a 'live' position of the wheel which enabled lifting the tyre to a 5cm height with precision and consistency. Height adjustments were made one minute after initial elevation to account for tensile deformation of the cable ties and to ensure the wheel/apparatus was not in motion. Cable ties were cut with pliers for instant release of the structure. Displacement, velocity, and accelerations were measured by the Vicon markers throughout the drop test. The vertical reaction force resulting from the tyre impact was recorded by the force plate.

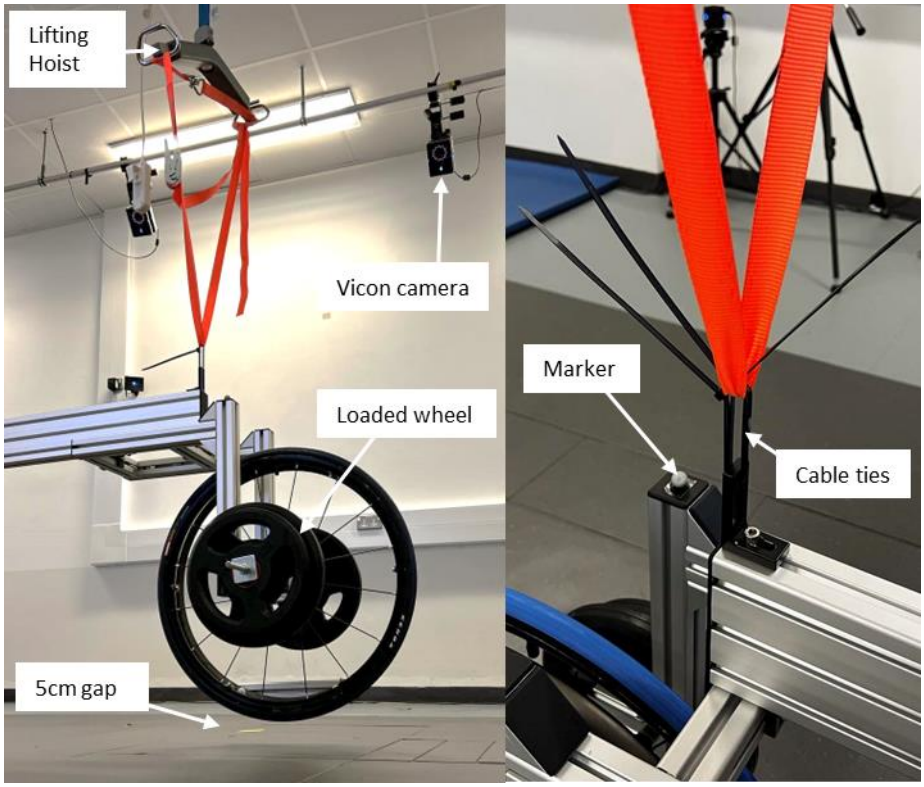

Figure 6 - Tyre testing rig setup for drop test. A mechanical lifting hoist elevated the beam and tyre via an attached strap. Vicon markers (positioned on the beam and at the tyre hub) recorded the position, velocity, and acceleration via several surrounding Vicon cameras. Cable ties cut with pliers enabled a quick release of the tyre, emulating a sudden drop (such as pavement dismount).

Identification of optimum spoke design for manufacturing

Material selection and manufacturing methods were used to inform the designs of the numerical models and are discussed in the next subsection (Development of a wheelchair FS-NPT prototype).

Finite Element (FE) analyses were conducted on Mechanical APDL 2021 R2 software to determine the behaviour of FS-NPTs with different spoke designs. For reference, a single spoke model of a honeycomb design, which had previously been found to be optimum over existing spoke designs (PhD research), was used (Figure 7). The upper and lower spoke layers (supports) had radius values assuming they belonged to a 24" FS-NPT that would fit onto the Fusion 16 spoke wheelchair wheel rim. The master node was positioned at the centre of this theoretical tyre and was coupled with the slave nodes situated on the top upper support via targe169 and conta172 contact elements respectively (using multi-point constraints). The whole model utilised 2D quadrilateral plane183 elements (higher order elements) with key option 'plane stress with thickness' (due to symmetrical geometry and loading). A mesh convergence concluded that a 0.2mm element size was required for independence of results from the mesh. A 1.5mm element size was used for the ground as only the reaction force data was recorded here (by the ground master node). The lower support and ground contact behaviour was simulated via a frictional contact with a coefficient of 0.7 (Ganniari-Papageorgiou et al., 2020), using conta172 and targe169 contact elements respectively. Non-linear,

hyperelastic thermoplastic polyurethane with a Shore A hardness of 95 was used for the spokes and supports, and the ground was set to have a virtually infinite stiffness for incompressibility ($E > 1 \times 10^{18}$).

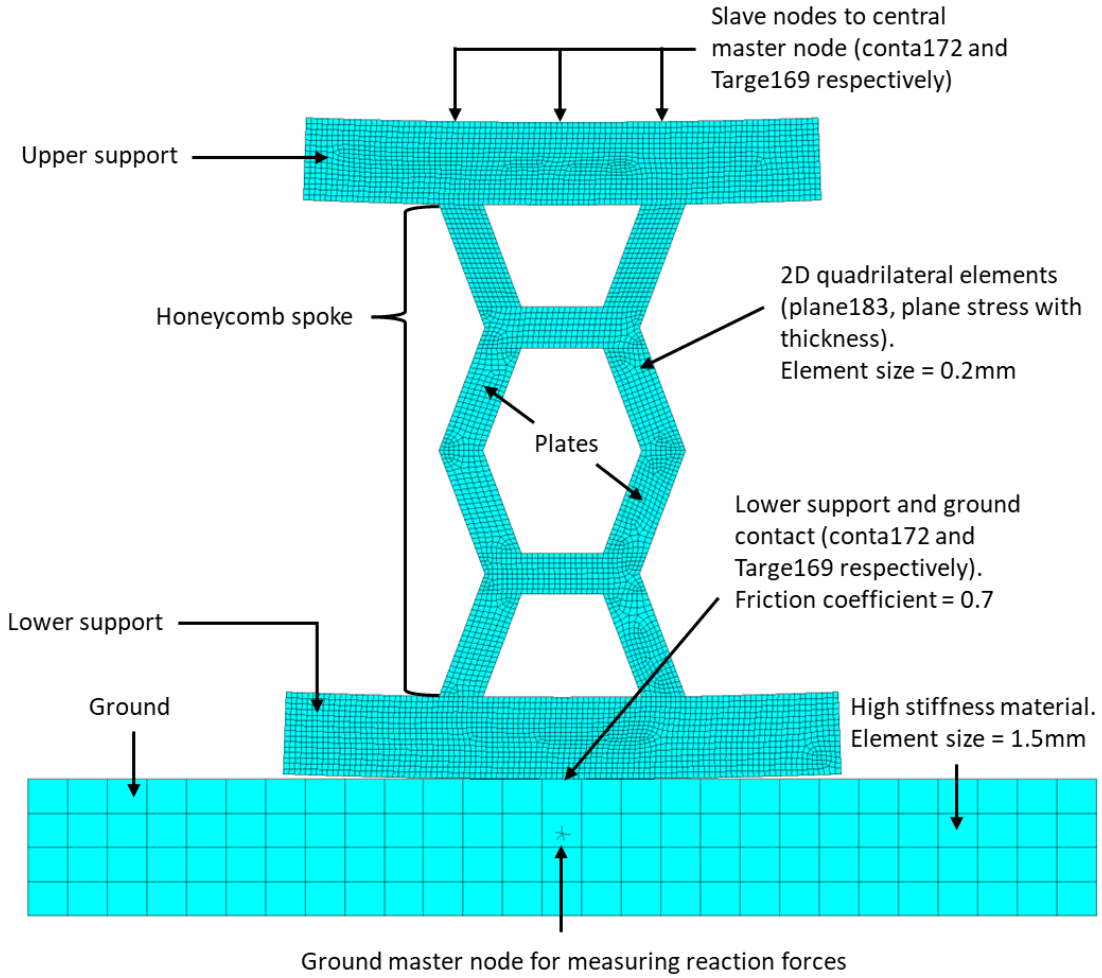

Figure 7 - FE model of a 2D single honeycomb spoke with identified features. Element and contact setup information is shown.

Vertical stiffness was measured by applying a vertical displacement to the central master node and measuring the sum of the vertical reaction forces recorded by the ground master node. Similar to the wheelchair tyre experiments, force – displacement graphs were produced (using data from simulation sub-steps). The initial slope of this graph was considered the average vertical stiffness, while equivalent vertical stiffness could be calculated for individual datapoints.

Post-buckling stiffness was also measured from the applied vertical displacement. The slope of the vertical stiffness after buckling initiation and high applied displacement was considered as the post-buckling stiffness.

Rotational stiffness was measured by first applying a vertical force equivalent to 80% of the buckling load of the particular spoke design (determined from the vertical stiffness simulation) (Chatzistergos & Chockalingam, 2021). Subsequently, a rotation (around the tyre depth axis, z) was applied to the central master node, and the sum of the parallel-to-ground reaction forces was recorded by the ground master node. Moment – rotation graphs were produced using this data, and the slope of this

graph was considered the average rotational stiffness, and equivalent rotational stiffness could be calculated for individual datapoints. To determine if a spoke exhibited different behaviour when rotated clockwise compared to counter-clockwise, the rotation was simply set to a negative value.

Including honeycomb, four reference designs were tested for the aforementioned mechanical properties. These were honeycomb, curved, triangular, and N-spoke (Figure 8). Except for honeycomb, these spokes were all unique and asymmetrical (in the tyre radial axis) and hypothesised to have adaptable vertical and rotational stiffnesses. The thickness of the plates and the supports of all designs was constant at 1.5mm and 3mm respectively. The height of all spokes (between supports) was also constant for all designs at 18mm.

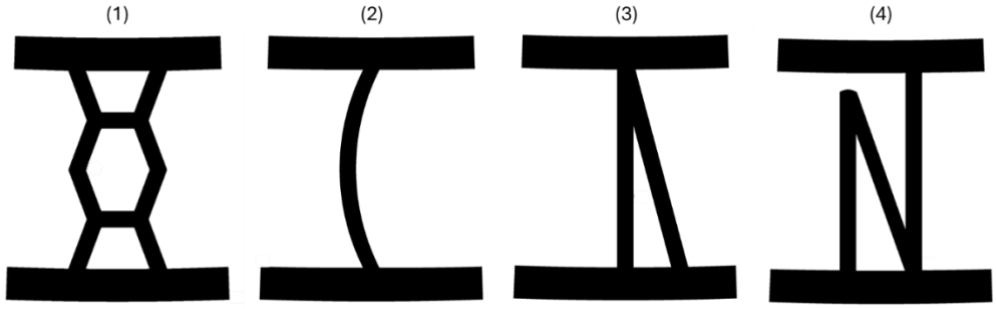

Figure 8 - Single spoke samples with varied spoke designs. (1) Honeycomb, (2) Curved, (3) Triangular, (4) N-spoke

Following the aforementioned FE process, step 1 of the analyses consisted of a large displacement of 5mm that was applied to the master node for each design to obtain sufficient force-displacement data and fully capture the spoke behaviours under compression. This was a standalone step in the analyses (Figure 9, step 1).

In step 2 part (a), a downward vertical force value of 80% relative to the buckling load (varies for each design) that was determined from step 1 was applied to the central master node, as this was deemed the maximum load before non-linear behaviour occurs (Chatzistergos & Chockalingam, 2021). In step 2 parts (b) and (c), in addition to the vertical force, a rotation was applied to the master node in the anti-clockwise and clockwise direction respectively.

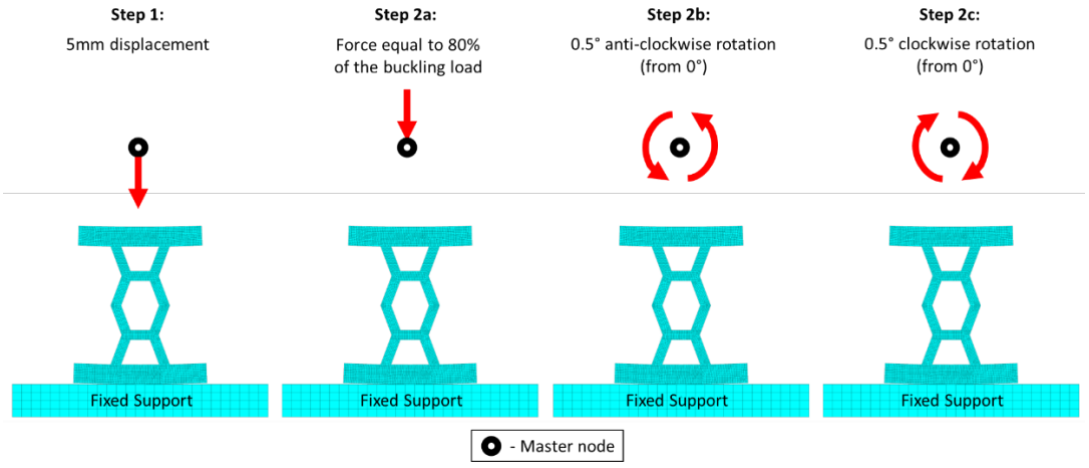

Figure 9 - Loading and constraints of the FE models

Honeycombs were chosen as the spoke design for the first prototype. The honeycomb design was chosen as this design had already been optimised for a 75kg wheelchair user using a Taguchi method and statistical model in supporting work. The structure was designed to remain within the initial stiffness region under the load of a user and was optimised to be as lightweight as possible. This design has therefore been proven to be numerically feasible. Initial samples were printed which proved that this design was indeed capable of being produced accurately via additive manufacturing. A whole FE honeycomb tyre model was created and simulated under the same loading conditions to obtain data that can be used in comparison with the prototype experimental testing results for validation (Figure 10).

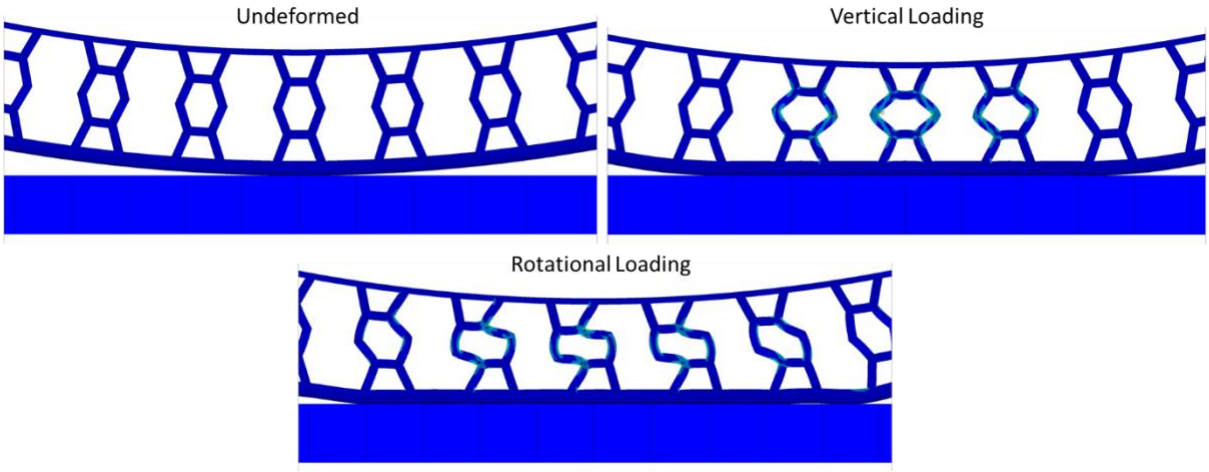

Figure 10 - Full honeycomb tyre showing the behaviour of the spokes during vertical and rotational loading equivalent to an average wheelchair users' weight and an average user's wheeling stroke.

Using preliminary FE results, a multi-layer perceptron regressor was used to predict outcome measures of the FE models. The data of outcome measures from 94 simulations of a full FS-NPT with a honeycomb design with randomly generated parameters (within specified ranges) were used to train the regressor. The network structure consisted of two hidden layers of 7 and 9 neurons. The squared error was specified as the loss function to be optimised (algorithms used were limited-memory Broyden-Fletcher-Goldfarb-Shanno and stochastic gradient descent).

Development of a wheelchair FS-NPT prototype

The structure of a typical non-pneumatic tyre consists of polymeric flexible spokes, a steel outer ring, and a rubber tread (Ganniari-Papageorgiou et al., 2020). The outer ring and tread are simple circular extrusions and therefore stock parts were attained from material/part suppliers. For the rubber tread, a neoprene rubber strip (15mm wide, 1.5mm thick, 5000mm length) was acquired and cut to size. For the steel outer ring, Jubilee clips (stainless steel slotted quick release strap: 11mm wide, 0.5mm thick, 1272mm length) were acquired.

The spokes of a non-pneumatic tyre are more complex in geometry and material and require an advanced manufacturing process. A review of relevant literature was conducted, and external manufactures were consulted to determine the current processes for manufacturing the spokes of

existing FS-NPTs. The three main manufacturing methods currently in practice are injection moulding, centrifugal casting, and 3D printing (Deng et al., 2023). Another process identified was subtractive machining from stock material. The method of identifying the spoke manufacturing process is briefly discussed below.

The advantages and disadvantages of the aforementioned manufacturing processes were assessed to determine the most suitable process. Whilst injection moulding and centrifugal casting can produce components of high quality and high strength respectively, they both require moulds which is not cost and time effective for prototype stages (Todd, Robert H and Allen, Dell K and Alting, 1994). Due to the typical materials used in the spokes of non-pneumatic tyres, machining was deemed unsuitable as it would likely cause flexing/stretching/tearing of the materials during the subtractive process.

On the other hand, 3D printing can design complex geometries efficiently in terms of time and cost, which makes it ideal for prototyping (Shahrubudin et al., 2019). Furthermore, 3D printers are widely accessible within universities and support compatibility with a broad range of materials, and therefore this manufacturing method was chosen to build the spokes. There are numerous 3D printing methods to choose from, and due to the typical materials used for the spokes in non-pneumatic tyres (soft polymers), Fused Deposition Modelling (FDM) was the method utilised to build them.

A review of materials was conducted and the university 3D printing flexible materials that were available were assessed. Due to availability, previous use, and validation, TPU95A was chosen as the material of the spokes. Other materials are planned to be analysed at later stages of this project.

The spokes were to be printed individually for modularity. As the honeycomb design usually has interconnecting plates, a simulation was conducted without the plates, and the design was manipulated to account for the decrease in stiffness (Figure 10). For the spokes to fit onto the Fusion 16 spoke wheelchair wheel, measurements of the internal area of the wheel rim were taken and preliminary samples were printed to determine the most appropriate size (Appendix 2), and Figure 11 shows the 3D printed design. The upper spoke layer was designed to accommodate the internal wheel rim area. To ensure that the spokes remained in place around the wheel, the upper support was designed so that once all the spokes had been put in place, there were no gaps between them. This was the same for the lower spoke layer. To hold the spokes tightly onto the wheel, a hole was designed in the upper spoke layers to accommodate a metallic wire (7x7 galvanised steel wire rope). This wire passed through all the spokes and into the wheel area via the pneumatic tyre inner tube valve hole. Here, the wire was held tightly using a wire tensioner (6mm hook/hook turnbuckle) and fasteners (1-2mm steel wire rope quick loop grips).

Finally, the outer ring was to be tightened via slotted screws and bonded to the lower spoke layers via a flexible urethane adhesive (URE-BOND II), and the rubber tread was to be bonded to the outer ring via the same adhesive, completing the FS-NPT.

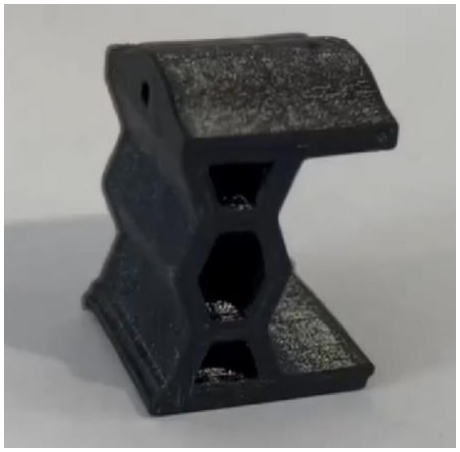

Figure 11 - TPU95A 3D printed honeycomb spoke. Upper area was designed to fit into the wheelchair wheel rim. A hole was designed to accommodate a wire to tightly hold it onto the wheel.

What we found

This section outlines the main findings of the project in subsections corresponding to the sections in the methodology.

Wheelchair tyre technology baseline mechanical behaviour

Table 2 contains the results of all 6 wheelchair tyres that were experimentally tested using the developed tyre testing rig (all data in Appendix 3). The tyre with the lowest vertical stiffness was the Cheng Shin pneumatic tyre which also had the lowest inflation pressure and was the heaviest, and the tyre with the highest vertical stiffness was the primo pneumatic tyre which was also the lightest. The solid tyres both had a similar rotational stiffness which was lower than all the pneumatic tyres at ≈88 Nm/°. The solid tyres had the highest peak reaction forces, and the pneumatic tyre with the lowest inflation pressure had the lowest peak reaction force. The solid tyres also deformed the least during impact at around 0.75mm, and the pneumatic tyre with the lowest inflation pressure had the highest deformation of 1.363mm.

Table 2 – All experimental wheelchair tyre testing results. S and P refer to solid and pneumatic respectively in the tyre type column.

	Tyre characteristics	Tyre characteristics	Tyre characteristics	5cm Drop Test	5cm Drop Test
Tyre Type:	Vertical Stiffness (kN/m)	Rotational Stiffness (Nm/°)	Mass (kg)	Peak Reaction Force (N)	Tyre Maximum Deformation (mm)
GreentyreA (S1)	128.6	87.2	0.498	-2533	-0.738
GreentyreB (S2)	141.8	88.6	0.558	-2643	-0.768
Primo (P1)	171.8	117.1	0.415	-2336	-1.122
Cheng Shin (P2)	108.8	108.7	0.613	-1920	-1.363
Schwalbe (P3)	130.9	95.4	0.606	-2233	-1.282
Kenda (P4)	150.8	126.9	0.422	-2365	-1.045

Graph 1 shows the three tests for vertical and rotational stiffnesses for pneumatic tyre 4 (Kenda) and is an example of how data was recorded and assessed. Graph 1a shows consistent results between retests. Graph 1b shows more diverging data points, but still a strong linear trend can be observed (moment starts at around 5Nm due to the attachable beam generating a small moment).

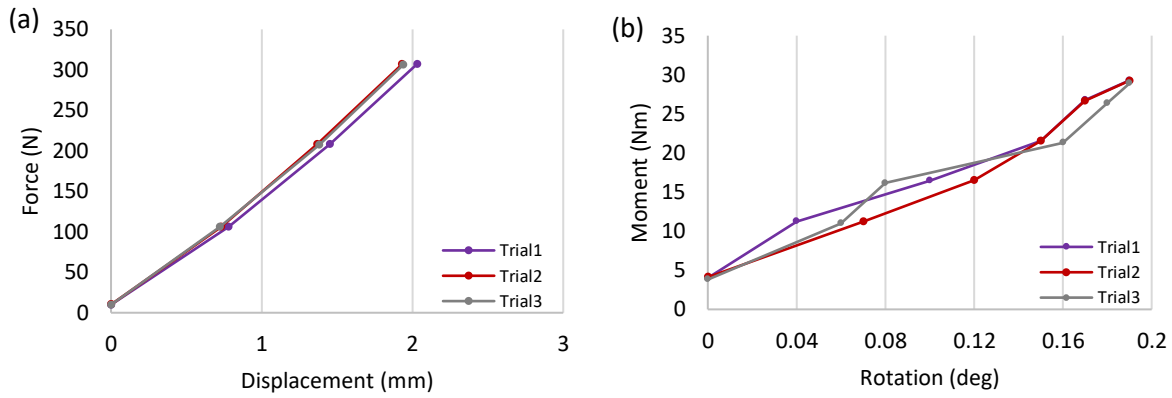

Graph 1 - Typical tyre testing results using pneumatic tyre 4 (P4) test data as an example. (a) Force – displacement graph of three individual trials; slope magnitude is equal to the vertical stiffness of the tyre. (b) Moment- rotation graph of three individual trials; slope magnitude is equal to the rotational stiffness of the tyre.

Graph 2 shows the typical response of the force plate during a drop test with a pneumatic tyre (a) and a solid tyre (b). The pneumatic tyre had a lower peak reaction force, which is common among all the pneumatic tyres compared to solid tyres. The force plate returning to zero after peak force indicates that the tyre is not in contact, and therefore has rebounded off the ground and is suspended in air. In this case, the pneumatic tyre rebounded approximately triple the number of times compared to the solid tyre and takes up to 2 seconds longer to settle after impact. This behaviour was similar for all pneumatic and solid tyres.

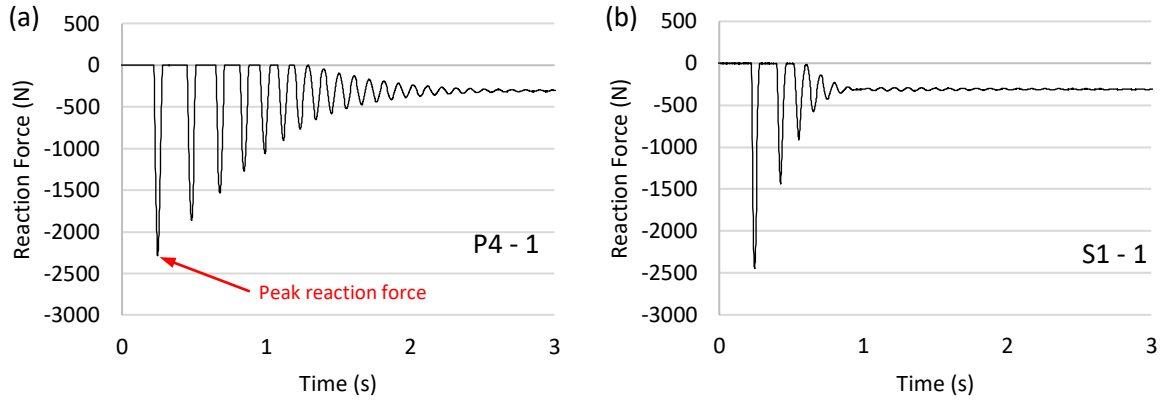

Graph 2 – Typical response of pneumatic and solid tyre vertical reaction force. Reaction force is always negative, and the graphs trail off to ≈300N which is the force from the weight of the tyre. (a) Reaction force-time graph for the drop test of pneumatic tyre 4 test 1 at 5cm height. (b) Reaction force-time graph for the drop test of solid tyre 1 test 1 at 5cm height.

Graph 3 shows the marker position placed at the wheel hub throughout the drop tests. As the cable ties were cut, the tyre fell until ground impact (0), and then deformation of the tyre occurred before

rebounding off the ground. The pneumatic tyre had higher deformation and rebounded approximately double the height of the solid tyre. This behaviour was similar for all pneumatic and solid tyres.

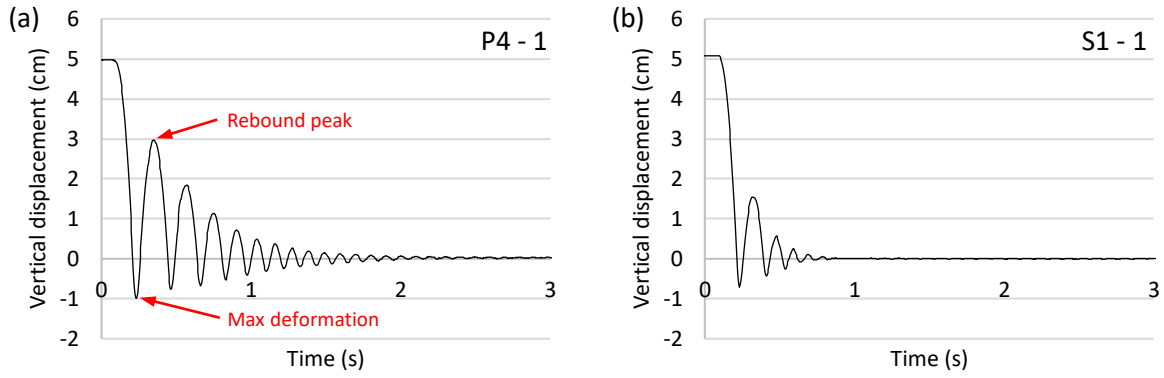

Graph 3 – Typical response of pneumatic and solid tyre vertical displacement with 5cm being the raised height of the tyre, and 0cm being the ground. Displacements below 0cm are tyre deformations. (a) Displacement-time graph for the drop test of pneumatic tyre 4 test 1 at 5cm height. (b) Displacement-time graph for the drop test of solid tyre 1 test 1 at 5cm height.

Graph 4 shows the vertical velocity of the marker at the wheel hub for a pneumatic (a) and solid (b) tyre. The speed of the tyre steadily increases (in the downward negative direction) until it contacts the ground (negative peak), and tyre deformation occurs resulting in reduced velocity until velocity reaches zero at maximum deformation. As the tyre undeforms, its velocity increases up until the point where it departs from the ground (positive peak). The velocity returns to zero as the tyre reaches its maximum rebound height. This process is repeated for each tyre rebound. Similar to the displacement results, the pneumatic tyre had many more peaks and troughs due to the increased number of rebounds from the ground compared to the solid tyre, and this was similar for all pneumatic and solid tyres. The negative peak velocity was the same for all tyres (dropped from the same height), and the peak positive velocities were significantly higher for the pneumatic tyres.

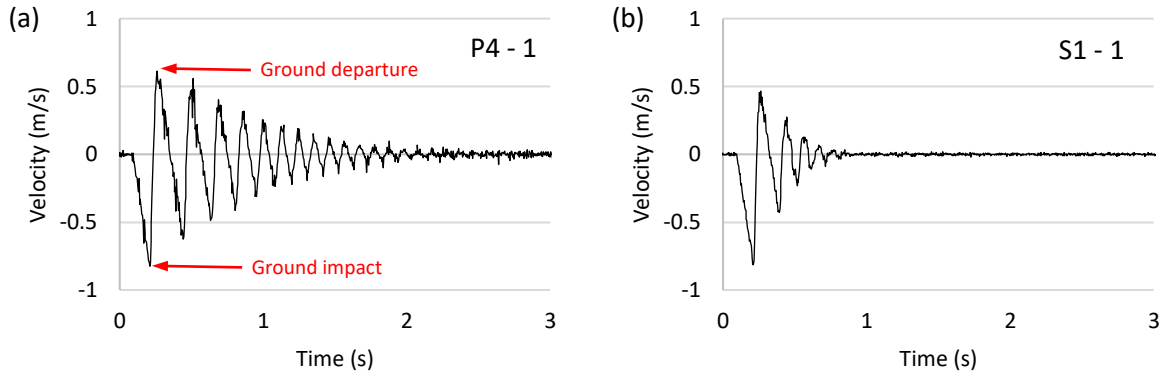

Graph 4 - Typical response of pneumatic and solid tyre vertical velocity. (a) Velocity-time graph for the drop test of pneumatic tyre 4 test 1 at 5cm height. (b) Velocity-time graph for the drop test of solid tyre 1 test 1 at 5cm height.

Graph 5 shows the vertical acceleration of the tyre marker for the pneumatic (a) and solid (b) tyres. Accelerations increased during impact and maximised around or just prior to tyre maximum deformation (the sensitivity and capture rate of the markers resulted in interference).

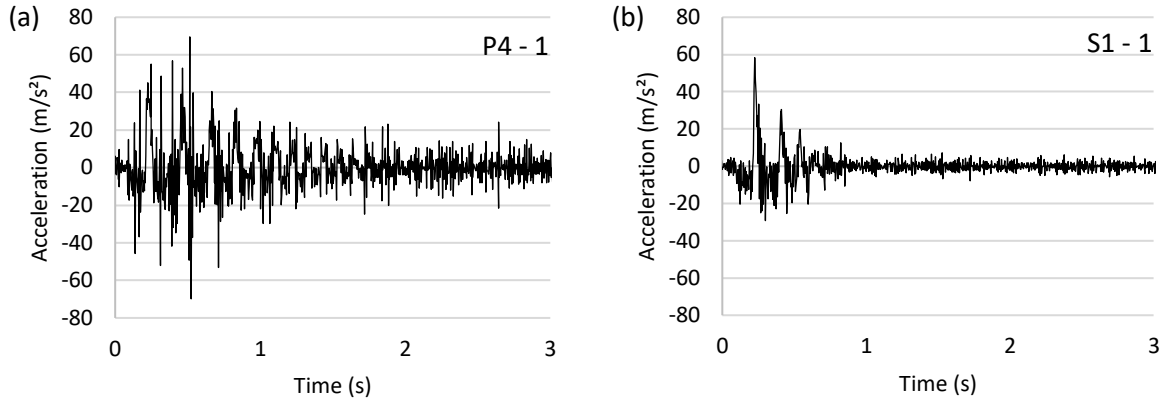

Graph 5 - Typical response of pneumatic and solid tyre acceleration. (a) Acceleration-time graph for the drop test of pneumatic tyre 4 test 1 at 5cm height. (b) Acceleration-time graph for the drop test of solid tyre 1 test 1 at 5cm height.

FS-NPT spoke design behaviour

Results of the FE single spoke models are presented here. Graph 6a shows the vertical load-displacement plotted data for the honeycomb design resulting from a 5mm applied displacement (step 1 of the FE loading steps). Key outcome measures are shown on the graph. Buckling load is defined as the point at which the structure either reaches a peak force or a large deviation from linearity occurs. In literature, 80% of the buckling load is stated to be where buckling initiates, and so behaviour prior to this is linear. The maximum linear load is shown at 80%, and this is the load that is applied in step 2a prior to applying rotations (this data is not shown as the graph would be a shorter version of Graph 6a). The initial stiffness (vertical) is defined as the stiffness up to this point (max displacement as this point is also recorded). The structure adopts a secondary stiffness after buckling occurs which is defined as the post-buckling stiffness. Graph 6b shows simulations steps 2b and 2c, which are the +0.5° and -0.5° applied rotations respectively and are subsequent to the applied vertical load equal to the maximum linear load (73.5N in this case). In Mechanical APDL software, anti-clockwise rotation is positive and will generate negative moment reaction forces, and vice versa. As the honeycomb design is symmetrical, the rotations are the same in either direction (and so propelling a wheelchair tyre with a symmetrical honeycomb design forwards and backwards would require the same exertion effort, like existing tyre technology). Also, due to symmetry, there are no moment reaction forces from the vertical load. Rotational stiffnesses are measured as the initial linear region slopes, and the moment values at the maximum applied rotations are recorded. Table 3 shows the data values of the outcome measures illustrated on Graph 6. These specific values cannot be compared to current wheelchair tyre technology as they are for a single spoke model only. However, their behaviour is representative of a complete FS-NPT with a multitude of spokes. Honeycomb had the largest displacement before buckling occurred compared to other designs (1.24mm).

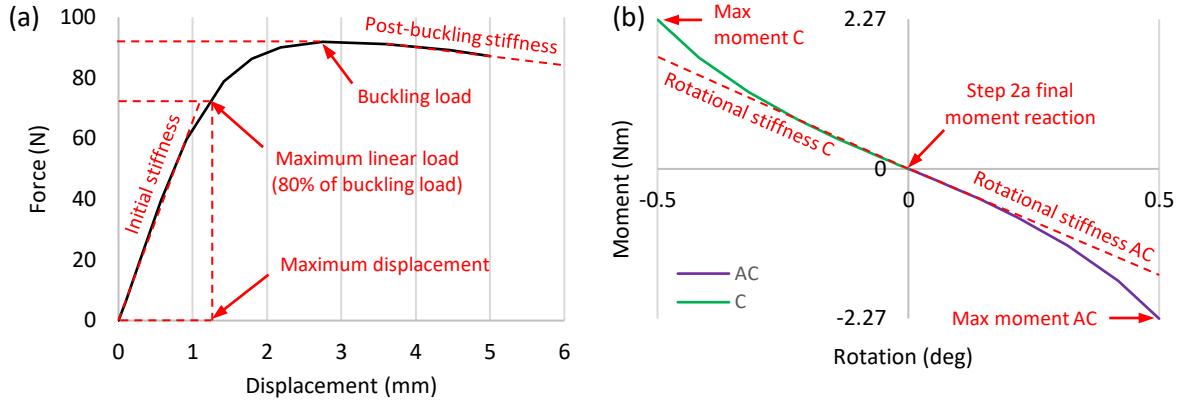

Graph 6 - Honeycomb single spoke FE plotted results. (a) Force-displacement graph for an applied 5mm displacement. (b) Moment-rotation graph for both applied rotations of 0.5° (AC) and -0.5° (C).

Table 3 - Honeycomb single spoke results from the applied FE loading steps (illustrated in honeycomb graphs). The moment values shown in parentheses are the difference from the step 2a final reaction moment, which is the change in moment reaction from rotation only.

						± 0.5° Rotation Results			
Step 1: 5mm Displacement Results			Step 2a: Vertical Loading Results			Step 2b: Anti-Clockwise (AC) Rotation		Step 2c: Clockwise (C) Rotation	
Initial Stiffness (kN/m)	Buckling Load (N)	Post-Buckling Stiffness (kN/m)	Max Linear Load (N)	Max Displacement (mm)	Final Moment Reaction (Nm)	Rotational Stiffness (Nm/°)	Maximum Moment (Nm)	Rotational Stiffness (Nm/°)	Max Moment (Nm)
66.4	91.9	-2.82	73.5	1.24	0	4.35	-2.27 (-2.27)	4.34	2.26 (2.26)

Graph 7a shows the force-displacement graph for the curved design. The behaviour is similar to the honeycomb design, although the initial stiffness region is short, and buckling occurs more gradually. Graph 7b shows the rotation and shows completely linear rotation in either direction up until the maximum applied rotations. The point at which the graph crosses the y-axis (step 2a final reaction moment) is not zero, indicating that reaction moments were generated during the applied vertical load only, which is due to asymmetric curvature of the design. Table 4 contains the curved spoke results. The curved spoke had the lowest initial vertical stiffness of all designs but is the only design with a positive post-buckling stiffness. Although the maximum moments vary, the actual change in moment during the rotation steps was negligible (0.003Nm difference).

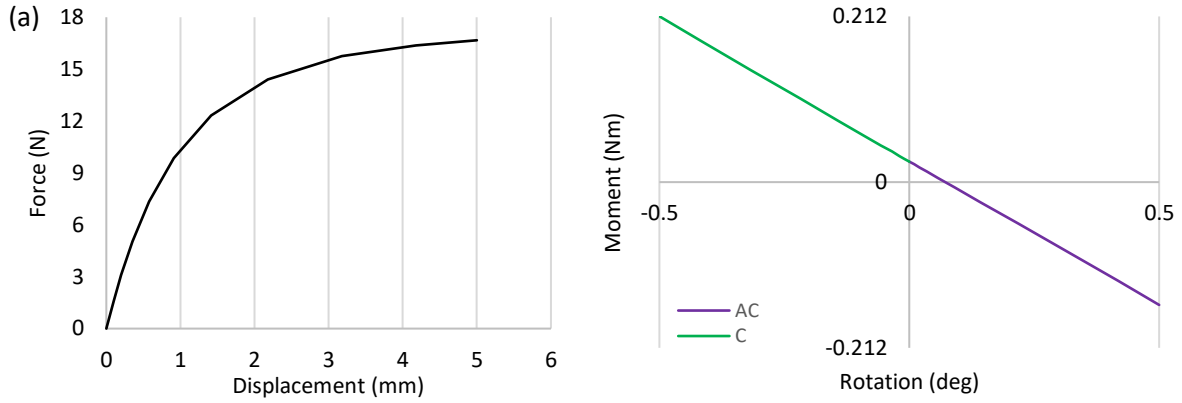

Graph 7 – Curved single spoke FE plotted results. (a) Force-displacement graph for an applied 5mm displacement. (b) Moment-rotation graph for both applied rotations of 0.5° (AC) and -0.5° (C).

Table 4 - Curved single spoke results from the applied FE loading steps.

						± 0.5° Rotation Results			
Step 1: 5mm Displacement Results			Step 2a: Vertical Loading Results			Step 2b: Anti-Clockwise (AC) Rotation		Step 2c: Clockwise (C) Rotation	
Initial Stiffness (kN/m)	Buckling Load (N)	Post-Buckling Stiffness (kN/m)	Max Linear Load (N)	Max Displacement (mm)	Final Moment Reaction (Nm)	Rotational Stiffness (Nm/°)	Maximum Moment (Nm)	Rotational Stiffness (Nm/°)	Max Moment (Nm)
10.7	12.3	0.511	10	0.934	0.0262	0.366	-0.157 (-0.183)	0.371	0.212 (0.186)

Graph 8a shows the force-displacement graph for the triangular design. The response of this design shows a steep initial slope, and then a clear buckling point at the peak and a subsequent reduction in stiffness.

Graph 8b shows the rotation results for the triangular design (to 0.4° only due to unconverging simulations). The rotational stiffness is linear for only small rotations, and then deviates from linearity, and this happens for a smaller rotation in the clockwise direction compared to anti-clockwise. The triangular design has the highest moment reaction from step 2a. Table 5 shows the results of the triangular design. The triangular design had the highest vertical stiffness of all designs but was the first to buckle in terms of displacement. It also had the highest negative post-buckling stiffness. The moment change during the clockwise rotation is almost double that of the anti-clockwise rotation moment. The rotational stiffnesses are also the lowest, but they become stiffer as rotation increases.

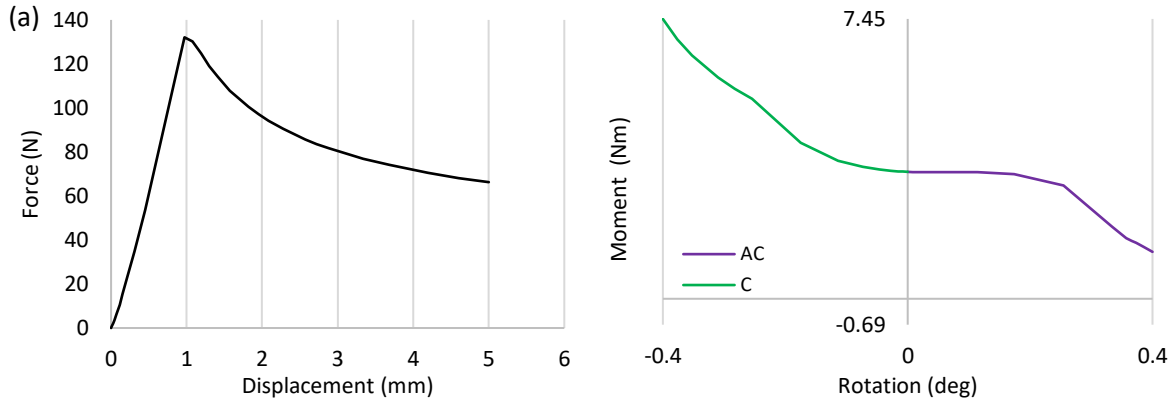

Graph 8 - Triangular single spoke FE plotted results. (a) Force-displacement graph for an applied 5mm displacement. (b) Moment-rotation graph for both applied rotations of 0.4° (AC) and -0.4° (C) (the FE simulations were unable to solve to 0.5° for the triangular spoke designs).

Table 5 - Triangular single spoke results from the applied FE loading steps.

						± 0.5° Rotation Results			
Step 1: 5mm Displacement Results			Step 2a: Vertical Loading Results			Step 2b: Anti-Clockwise (AC) Rotation		Step 2c: Clockwise (C) Rotation	
Initial Stiffness (kN/m)	Buckling Load (N)	Post-Buckling Stiffness (kN/m)	Max Linear Load (N)	Max Displacement (mm)	Final Moment Reaction (Nm)	Rotational Stiffness (Nm/°)	Maximum Moment (Nm)	Rotational Stiffness (Nm/°)	Max Moment (Nm)
135.1	132.1	-9.28	106	0.796	3.38	0.268	1.29 (2.13)	1.42	7.45 (4.07)

Graph 9a shows the vertical force-displacement graph for the 'N' single spoke design. This design is unique in that it has two buckling points. The structure buckles and shortly afterwards, the corner of the 'N' makes contact with the upper support which improves the structures stability and linearity returns. After further loading, it buckles again up to a point where internal contacts are made (plate to plate) which increases the stiffness of the structure. Graph 9b shows the rotation of the triangular design. The second buckling point was taken as the buckling load with the aim that tuning could allow the first buckling to occur when a person sits in their wheelchair, and the second when they dismount a pavement. Anti-clockwise rotation is linear, but clockwise direction produces a negative rotational stiffness. It appears that rotating the triangle clockwise causes the secondary buckling to occur (Appendix 4).

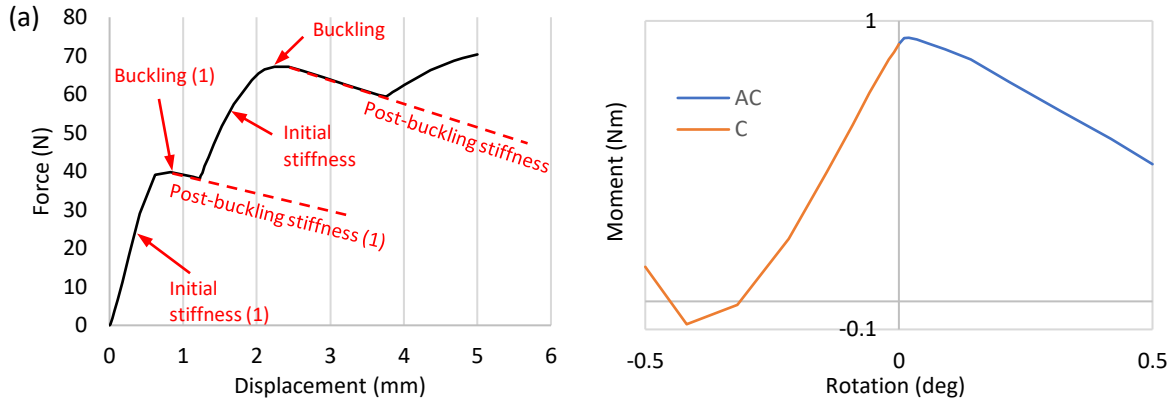

Graph 9 - N-spoke single spoke FE plotted results. (a) Force-displacement graph for an applied 5mm displacement. Buckling is observed twice, and the second buckling load was used to define the max linear load. (b) Moment-rotation graph for both applied rotations of 0.5° (AC) and -0.5° (C).

Table 6 – N-spoke single spoke results from the applied FE loading steps.

						± 0.5° Rotation Results			
Step 1: 5mm Displacement Results			Step 2a: Vertical Loading Results			Step 2b: Anti-Clockwise (AC) Rotation		Step 2c: Clockwise (C) Rotation	
Initial Stiffness (kN/m)	Buckling Load (N)	Post-Buckling Stiffness (kN/m)	Max Linear Load (N)	Max Displacement (mm)	Final Moment Reaction (Nm)	Rotational Stiffness (Nm/°)	Maximum Moment (Nm)	Rotational Stiffness (Nm/°)	Max Moment (Nm)
72.7 / 42.8	39.8 / 67.1	-4.06 / -6.07	54	0.464 / 1.71	0.917	0.951	0.489 (0.428)	-3.02	0.123 (0.794)

For the entire honeycomb FS-NPT, the design was tuned (through altering number of spokes and angle of the internal plates) to have the same displacement as the pneumatic tyres tested (averaged) as these tyres generally have better cushioning and wheeling efficiency. The maximum displacement of the honeycomb model with an applied vertical load of 306N was 2.09mm (within 1% of the wheelchair pneumatic tyre displacements), meaning it had a vertical stiffness of 146 kN/m. A 25 Nm moment (applied in the tyre rotational experiments) was subsequently applied as a second load step and the resultant rotation was 0.0487°, meaning it had a rotational stiffness of 513 Nm/°. Comparing this with the wheelchair conventional tyre experiments, the vertical stiffness is within the range of all tyre vertical stiffnesses, and the rotational stiffness appears to be significantly higher in the FS-NPT numerical model. These numerical values can also be directly compared with the vertical and rotational tyre testing experiments for the FS-NPT prototype (future work).

The results of the multi-layer perceptron regressor indicated that 4500 iterations were required for convergence of results during the training process. The regressor was capable of predicting the vertical stiffness with an accuracy of 96.3%.

FS-NPT prototype

Figure 12 shows the first of its kind FS-NPT with a honeycomb spoke design manufactured for a manual wheelchair. 105 honeycomb spokes are shown that are well-connected around the wheel. This wheel was able to be mounted onto the frame of a standard active manual wheelchair (RGK Hi-Lite Titanium), shown in Figure 13. A solid tyre was used on the other wheel, and the wheelchair remained level and balanced during rolling. The tyre brake was effective, and the tyre did not interfere with propulsion. Figure 14 shows a close view of the spokes.

The total cost of the 3D printing, including the 105 spokes, spare spokes, and initial samples (to test the wire hole, wheel rim shape, thickness of supports etc.) was approximately £60. The other parts needed to assemble the tyre were of low cost, meaning that the full tyre cost less than £70 to manufacture (not including the price of the glue).

The tyre weighed 0.513 kg which puts it in the middle of the weight of the 6 wheelchair tyres. The tyre has the potential to lose further weight by removing the turnbuckle and fixing the wires elsewhere.

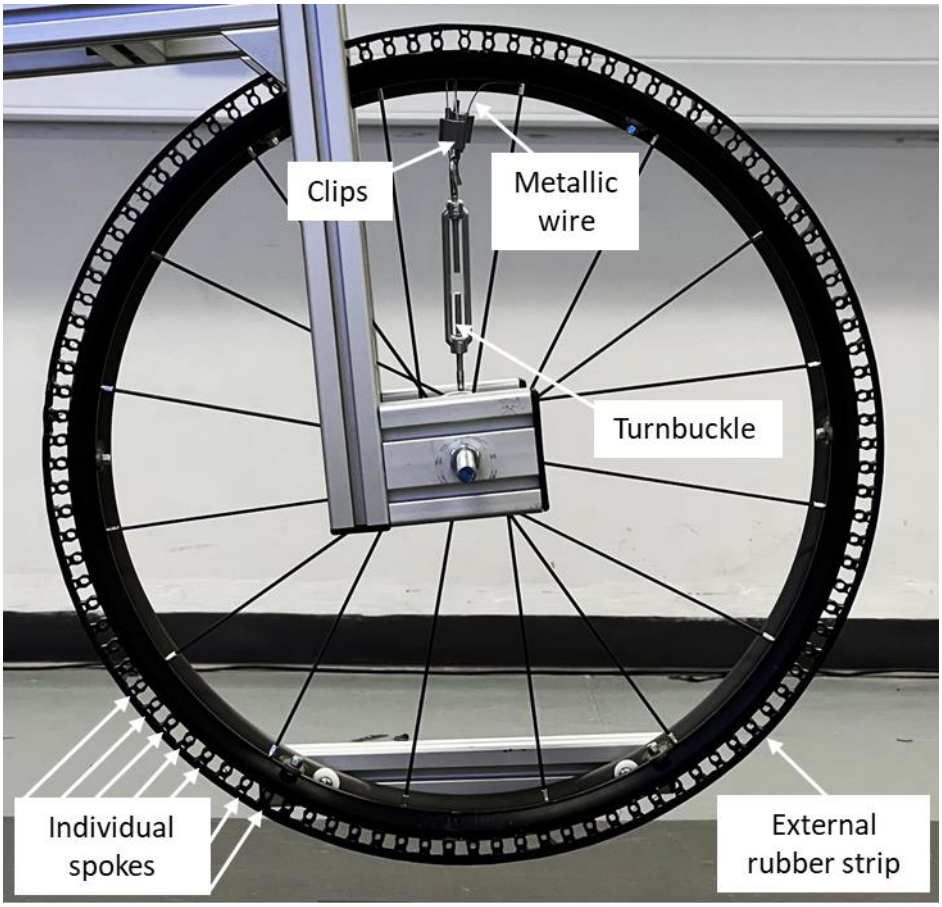

Figure 12 - The first manufactured prototype of an FS-NPT for wheelchairs utilising honeycomb spokes.

Figure 13 - The first wheelchair FS-NPT mounted onto an active wheelchair (RGK Hi-Lite Titanium)

Figure 14 - Close up of the spokes belonging to the wheelchair FS-NPT.

What this means

Vertical stiffness of current wheelchair tyre technology ranges from 108.8 to 171.8 kN/m. The lowest and highest stiffness both belong to pneumatic tyres, indicating that the inflation pressure of pneumatic tyres can be used to tune the tyre to become stiffer or softer than solid tyres. As the vertical stiffness of a tyre is a key outcome measure that defines its behaviour, a tyre with a vertical stiffness within this range would likely be wheelchair compatible. However, an important feature which correlates to user comfort is a tyre's ability to absorb impact forces such as from pavement dismounts. A low peak reaction force indicates that the tyre has absorbed some of the impact through deformation, which is vital for improving comfort and the quality of life of wheelchair users. The vertical stiffness tests indicate that deformation was similar across all tyres, but the pneumatic tyres deformed significantly more for the drop tests, indicating that the viscoelastic behaviour of the tyres could be playing a key role in providing comfort.

All wheelchair tyres tested indicated virtually linear results in both vertical and rotational tests. The numerical testing of the spoke designs firstly indicated that FS-NPTs can exhibit a wide range of mechanical behaviours. All designs demonstrated adaptable stiffnesses in the vertical loading scenarios which has been proven to be unavailable in current tyre technology in this study. Previous work has proven that altering the geometry of spokes can tune the mechanical behaviour, and one such way is to increase the thickness of the spokes to increase the stiffness. Applying this to these spoke designs can enable altering the load required to buckle and therefore the load equivalent to stiffness adaptation. Not only can this be used to adapt to different loading scenarios, but it can also be used to tune to a user's specific weight. Furthermore, different spoke designs have demonstrated varied mechanical behaviour, and it could be that there is not one design that fits all, but a variety of

designs are needed to encompass the broad range of needs of wheelchair users. For instance, as triangular was the stiffest vertically, this may be optimal for users with a higher weight, whereas a user who desires minimal exertion, the honeycomb design may be best due to its high rotational stiffness.

In terms of rotational stiffness, two of the asymmetric designs (triangular and N-spoke) showed differences in reaction moments when rotating in different directions. The N-spoke utilised buckling to give a negative moment reaction. If this was tuned correctly, with a specified amount of force, the tyre could become softer and 'deflate' seemingly by itself during the braking process, thus improving braking efficiency. On the other end of this, exhibiting behaviour similar to Graph 9b, the tyre would have higher rotational stiffness when propelling forwards, resulting in a tyre that is more responsive and manoeuvrable.

The prototype FS-NPT was successfully assembled using a modular design. This was done via 3D printing of the individual spokes. Firstly, this manufacturing process enabled the printing to be done at the university and could even be extended to people who own a printer being able to print their tyres at home. Either way, this avoided the need for an external manufacturer which would likely have been complex and potentially expensive and timely to manufacture the tyre. Whilst the tyre may seem expensive initially (≈£70), the longevity of this tyre as a result of its puncture proofness and modular design allowing replacement of individual damaged spokes means that the tyre should be cost effective over time. Furthermore, mass production would also reduce manufacturing costs.

Overall, this study has demonstrated that an FS-NPT with modular design is capable of being mounted onto existing wheelchair wheels. Also, FS-NPT spoke designs can be used to adapt tyre stiffnesses to ever day loading scenarios such as pavement dismount and tyre propulsion and braking. The findings of this study have been shared with wheelchair users involved in the project and this collaboration is intended to continue and expand as this research develops. All internal and external group meetings were held online to minimise carbon impact.

What next

The next stages of this study will involve laboratory testing of the manufactured FS-NPT prototype. The experimental results of the conventional tyre technology will be used to assess the feasibility of the FS-NPT and to also assess its potential for improved performance through direct comparison. More specifically, this will involve assessing whether the FS-NPT prototype is capable of replicating similar vertical stiffnesses to conventional pneumatic tyres (for feasibility), and to assess whether it can achieve a higher rotational stiffness (for ease of wheeling), as well as a lower mass. Furthermore, assessing whether an FS-NPT can adapt its stiffness and provide increased cushioning during wheelchair users' regular daily tasks such as pavement/kerb dismount is important for reducing musculoskeletal pain to users and improving quality of life. This can be achieved by measuring the peak reaction forces and tyre deformation during the dynamic drop tests and comparing with conventional tyre technology. The experimental results of the FS-NPT prototype will also enable optimising entire FS-NPT models which can be combined with machine learning algorithms to predict the behaviour of the tyre without the need for FE modelling. The multi-layer perceptron regressor proved to be 96.3% accurate in predicting the vertical stiffness of an FS-NPT. Further data collection and analysis can help produce a more robust regressor capable of predicting multiple outcome

measures with increased accuracy, eliminating the FE step in the production of wheelchair FS-NPTs and allowing for its ease of use in industry and other settings where FE expertise is unavailable.

Our ambition is to maximise societal impact by producing a unique wheelchair tyre technology that can be widely adopted and used to improve the quality of life of wheelchair users. This project is a major steppingstone in this direction because it will unlock funding opportunities that are not currently available for this project, and significantly enhance chances of success. More specifically, this project will enable the validation of basic science and key concepts of the proposed technology in the laboratory (Technology Readiness Level 3), thus unlocking access to InnovateUK funding. InnovateUK's focus on the development of new products/services is a perfect alignment with the aims and goals of this project. Moreover, the evidence about the feasibility and the potential benefits of the proposed technology that has been collected as part of this project, will enable effective engagement with industry and enhance our chances for attracting direct investment.

In terms of impact, an FS-NPT feasibility publication has recently been submitted to the Scientific Reports journal titled "A Flexible-Spoke Non-Pneumatic Tyre for Manual Wheelchairs". Another publication is in preparation regarding the mechanical testing for the baseline properties of wheelchair tyres; the targeted journal for this publication is Medical Engineering and Physics. A third publication is planned to follow on the prototyping elements of this study combined with the aforementioned planned future work. This will include the mechanical testing of the wheelchair FS-NPT and will involve in-vivo testing with wheelchair users. This goes beyond the scope of this grant but is achievable with minimal support; options are currently being explored to support this work. All key findings will also be shared through social media and online platforms. The creation of high-quality material (images of research, videos) will be commissioned to support dissemination. Communication beyond the scientific community will be supported by our PPIE group.

References

Chatzistergos, P. E., & Chockalingam, N. (2021). A novel concept for low-cost non-electronic detection of overloading in the foot during activities of daily living. *Royal Society Open Science*, *8*(6). https://doi.org/10.1098/rsos.202035

Cowan, R. E., Fregly, B. J., Boninger, M. L., Chan, L., Rodgers, M. M., & Reinkensmeyer, D. J. (2012). Recent trends in assistive technology for mobility. *Journal of NeuroEngineering and Rehabilitation*, *9*(1), 1–8. https://doi.org/10.1186/1743-0003-9-20

Deng, Y., Wang, Z., Shen, H., Gong, J., & Xiao, Z. (2023). A comprehensive review on non-pneumatic tyre research. *Materials and Design*, *227*(February), 111742. https://doi.org/10.1016/j.matdes.2023.111742

Dinato, R. C., Ribeiro, A. P., Butugan, M. K., Pereira, I. L. R., Onodera, A. N., & Sacco, I. C. N. (2015). Biomechanical variables and perception of comfort in running shoes with different cushioning technologies. *Journal of Science and Medicine in Sport*, *18*(1), 93–97. https://doi.org/10.1016/j.jsams.2013.12.003

Dorfi, H. R. (2004). Tire cleat impact and force transmission: Modeling based on FTIRE and correlation to experimental data. *SAE Technical Papers*, *724*. https://doi.org/10.4271/2004-01-1575

Dudziak, M., Lewandowski, A., & Waluś, K. J. (2020). Static tests the stiffness of car tires. *IOP Conference Series: Materials Science and Engineering*, *776*(1). https://doi.org/10.1088/1757-899X/776/1/012071

Flemmer, C. L., & Flemmer, R. C. (2016). A review of manual wheelchairs. *Disability and Rehabilitation: Assistive Technology*, *11*(3), 177–187. https://doi.org/10.3109/17483107.2015.1099747

Ganniari-Papageorgiou, E., Chatzistergos, P., & Wang, X. (2020). The Influence of the Honeycomb Design Parameters on the Mechanical Behavior of Non-Pneumatic Tires. *International Journal of Applied Mechanics*, *12*(3). https://doi.org/10.1142/S1758825120500246

Gent, A. N., & Walter, J. D. (1977). Pneumatic tire. *Composites*, *8*(4), 271. https://doi.org/10.1016/0010-4361(77)90231-2

Initiative, M. I. T. D. C. (2019). *Wheelchair Evaluation MIT D-Lab Comprehensive Initiative on Technology Evaluation Massachusetts Institute of Technology*. *September*.

ISO. (2014). *ISO 7176-8 - Wheelchairs - Part 8: Requirements and test methods for static, impact and fatigue strengths*. https://www.iso.org/standard/64902.html#:~:text=ISO 7176-8%3A2014 specifies requirements for static%2C impact%2C and,specifies requirements for disclosure of the test results.

Koontz, A. M., Cooper, R. A., Boninger, M. L., Yang, Y., Impink, B. G., & Van Der Woude, L. H. V. (2005). A kinetic analysis of manual wheelchair propulsion during start-up on select indoor and outdoor surfaces. *Journal of Rehabilitation Research and Development*, *42*(4), 447–458. https://doi.org/10.1682/JRRD.2004.08.0106

Mason, B., Warner, M., Briley, S., Goosey-Tolfrey, V., & Vegter, R. (2020). Managing shoulder pain in manual wheelchair users: a scoping review of conservative treatment interventions. *Clinical Rehabilitation*, *34*(6), 741–753. https://doi.org/10.1177/0269215520917437

Mclaurin, C. A., & Brubaker, C. E. (1991). Biomechanics and the wheelchair. *Prosthetics and Orthotics International*, *15*(1), 24–37. https://doi.org/10.3109/03093649109164272

Rodrigo, S. E., & Herrera, C. V. (2018). Chapter 11 - Wheelchairs: history, characteristics, and technical specifications. In *Chiral Analysis* (Second Edi). Elsevier B.V. https://doi.org/10.1016/B978-0-12-812892-3/00011-X

Sawatzky, B. J., Kim, W. O., & Denison, I. (2004). The ergonomics of different tyres and tyre pressure during wheelchair propulsion. *Ergonomics*, *47*(14), 1475–1483. https://doi.org/10.1080/00140130412331290862

Shahrubudin, N., Lee, T. C., & Ramlan, R. (2019). An overview on 3D printing technology: Technological, materials, and applications. *Procedia Manufacturing*, *35*, 1286–1296. https://doi.org/10.1016/j.promfg.2019.06.089

Sonenblum, S. E., Sprigle, S. H., & Martin, J. S. (2016). Everyday sitting behaviour of full-time wheelchair users. *Journal of Rehabilitation Research and Development*, *53*(5), 585–598.

Todd, Robert H and Allen, Dell K and Alting, L. (1994). Manufacturing processes reference guide. *Industrial Press Inc.* https://books.google.co.uk/books?hl=en&lr=&id=6x1smAf_PAcC&oi=fnd&pg=PR9&dq=casting+manufacturing+processes&ots=g1VpA-oa44&sig=YylL5hrGnKqxxmZD4XUCeNIVzEU&redir_esc=y#v=onepage&q=casting manufacturing processes&f=false

WHO. (2008). *Guidelines on the provision of manual wheelchairs in less resourced settings*.

World. (2017). *Wheelchair publications - an overview*. https://www.who.int/news-room/articles-detail/wheelchair_publications–an_overview#:~:text=However%2C the World Health Organization.

Wyatt, O., Chatzistergos, P., Ganniari-Papageorgiou, E., & Chockalingam, N. (2021). A Finite Element Investigation into the Tunability of Non-Pneumatic Tyres for Wheelchair Use. *ISb2021*, *PC021*, 784. isb2021_programabstracts.pdf (isbweb.org)

Zmuda, M., Jackowski, J., & Hryciów, Z. (2019). Numerical research of selected features of the non-pneumatic tire. In B. P., S. A., & K. P. (Eds.), *15th Conference on Computational Technologies in Engineering, TKI 2018* (Vol. 2078). American Institute of Physics Inc. https://doi.org/10.1063/1.5092030

Appendix

Appendix 1: Tyre Testing Rig Concepts

Concept 1:

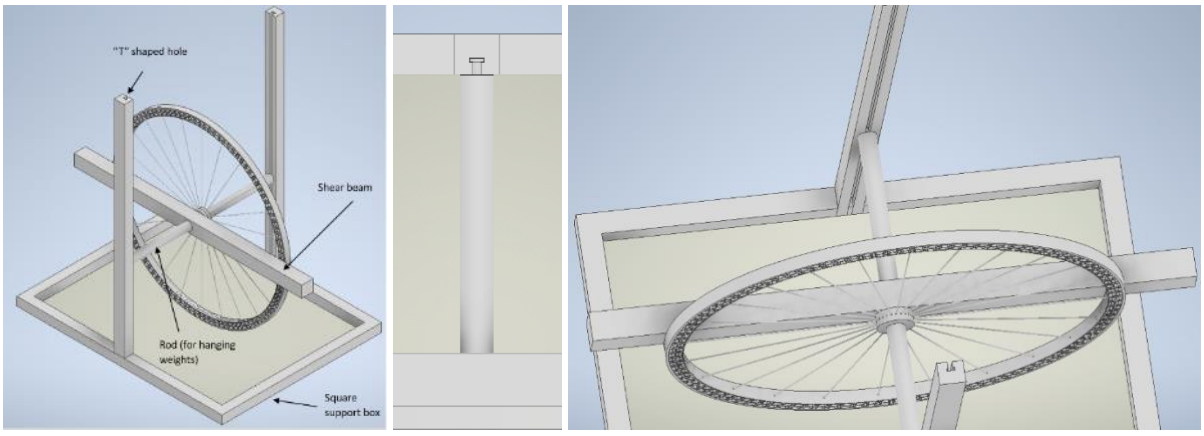

This initial tyre testing rig concept comprised a rod that would be positioned through the centre of the wheel. This rod would be attached to vertical beams on either side which have a ‘T’ shaped negatives and the rod would have “T” shaped positives on either side to allow the rod to fit inside these beams (from above) and be moved down until the tyre touches the floor. It is therefore constrained to the

vertical direction which can be used for the drop test. The rod could also be used to hang weights from to apply the vertical load. A shear beam could also be attached which can be drilled to allow the rod to pass through. Weights can also be hung from the shear beam to apply a rotational load. The structure has a square base support to hold it rigidly in place.

A limitation of this concept was that the 'T' shaped gaps would have had to be precisely engineered to match the 'T' shaped extrusions of the rod to minimise wobbling and friction during the tyre drop test. It was also realised that any weight imbalances in the wheel or dropping the wheel at a slight angle would cause the rod to get stuck on one side, rendering the drop test ineffective.

Appendix 2: Trialling inner wheel size

The outer rim of the Fusion 16 spoke wheelchair wheel was not a flat surface. To ensure that the manufactured spoke samples did not compress inside this gap and cause undesirable behaviour, several samples were printed to determine the correct fitting. A curvature with a 2.5mm height had the best fit.

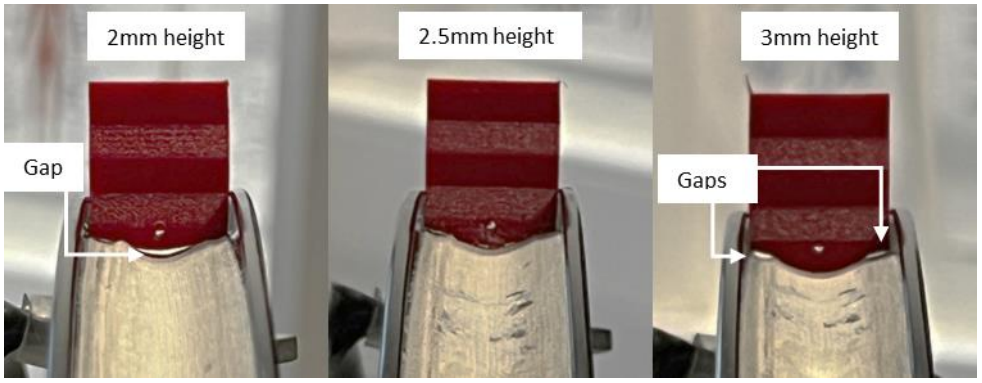

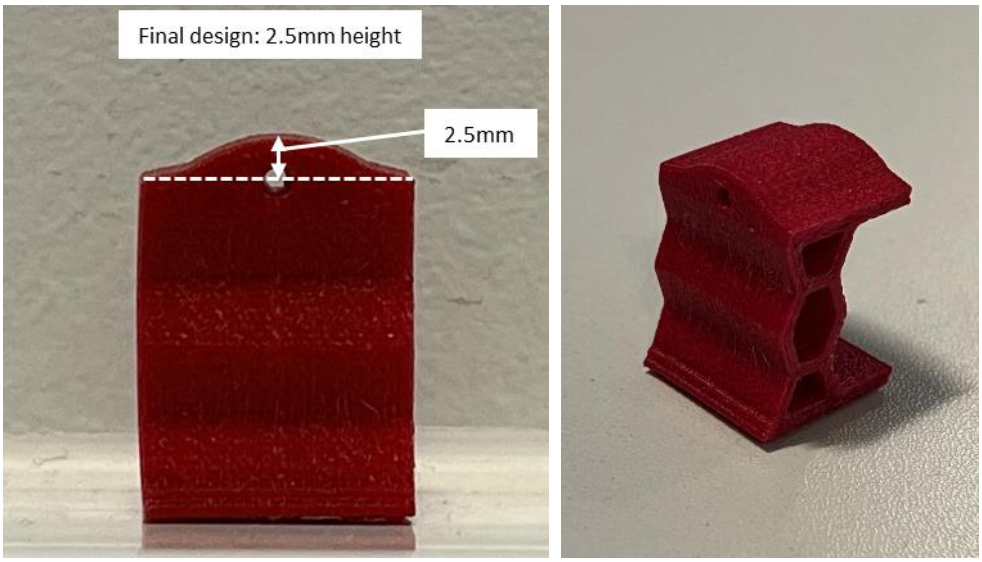

Appendix 3: All tyre testing results

SOLID TYRE 1 (S1)	Mechanical Characterisitcs		5 cm Drop Test					
Test Number	Vertical Stiffness (kN/m)	Shear Stiffness (Nm/°)	Peak Reaction Force (N)	Tyre Maximum Deformation (mm)	Minimum Velocitiy (m/s)	Maximum Velocitiy (m/s)	Minimum Acceleration (m/s²)	Maximum Acceleration (m/s²)
1	124.807	93.586	-2443.620	-0.708	-0.814	0.466	-29.188	58.308
2	126.525	86.042	-2554.790	-0.747	-0.811	0.440	-62.404	61.602
3	134.358	81.928	-2601.730	-0.760	-0.846	0.434	-35.101	59.603
Average:	128.563	87.186	-2533.380	-0.738	-0.824	0.446	-42.231	59.838
Standard Deviation	5.092	5.912	81.200	0.027	0.019	0.017	17.719	1.660
Coefficient of Variation (%)	3.960	6.781	-3.205	-3.705	-2.355	3.811	-41.957	2.774

SOLID TYRE 2 (S2)	Mechanical Characterisitcs		5 cm Drop Test					
Test Number	Vertical Stiffness (kN/m)	Shear Stiffness (Nm/°)	Peak Reaction Force (N)	Tyre Maximum Deformation (mm)	Minimum Velocitiy (m/s)	Maximum Velocitiy (m/s)	Minimum Acceleration (m/s²)	Maximum Acceleration (m/s²)
1	131.681	85.930	-2396.260	-0.716	-0.808	0.437	-97.998	150.616
2	144.286	91.915	-2685.450	-0.775	-0.819	0.472	-111.547	114.649
3	149.365	88.018	-2846.030	-0.816	-0.874	0.705	-57.616	122.673
Average:	141.777	88.621	-2642.580	-0.769	-0.833	0.538	-89.054	129.312
Standard Deviation	9.105	3.038	227.929	0.050	0.035	0.146	28.056	18.880
Coefficient of Variation (%)	6.422	3.428	-8.625	-6.523	-4.225	27.085	-31.504	14.600

PNEUMATIC TYRE 1 (P1)	Mechanical Characterisitcs		5 cm Drop Test					
Test Number	Vertical Stiffness (kN/m)	Shear Stiffness (Nm/°)	Peak Reaction Force (N)	Tyre Maximum Deformation (mm)	Minimum Velocitiy (m/s)	Maximum Velocitiy (m/s)	Minimum Acceleration (m/s²)	Maximum Acceleration (m/s²)
1	177.6776994	116.2407407	-2338.700	-1.119	-0.815	0.714	-92.172	92.120
2	169.5735608	111.3085714	-2318.650	-1.170	-0.887	0.779	-98.559	80.662
3	168.1627174	123.7345538	-2350.850	-1.077	-0.829	0.662	-95.155	83.699
Average:	171.805	117.095	-2336.067	-1.122	-0.844	0.718	-95.296	85.494
Standard Deviation	5.135	6.257	16.261	0.046	0.038	0.058	3.196	5.936
Coefficient of Variation (%)	2.989	5.343	-0.696	-4.137	-4.505	8.142	-3.354	6.944

PNEUMATIC TYRE 2 (P2)	Mechanical Characterisitcs		5 cm Drop Test					
Test Number	Vertical Stiffness (kN/m)	Shear Stiffness (Nm/°)	Peak Reaction Force (N)	Tyre Maximum Deformation (mm)	Minimum Velocitiy (m/s)	Maximum Velocitiy (m/s)	Minimum Acceleration (m/s²)	Maximum Acceleration (m/s²)
1	111.993	104.533	-1852.620	-1.313	-0.871	0.823	-163.442	78.391
2	110.764	109.589	-1941.810	-1.398	-0.941	0.719	-127.788	94.216
3	103.565	112.101	-1966.100	-1.378	-0.834	0.708	-68.905	63.060
Average:	108.774	108.741	-1920.177	-1.363	-0.882	0.750	-120.045	78.556
Standard Deviation	4.553	3.855	59.753	0.044	0.054	0.063	47.742	15.579
Coefficient of Variation (%)	4.186	3.545	-3.112	-3.239	-6.169	8.454	-39.770	19.832

PNEUMATIC TYRE 3 (P3)	Mechanical Characterisitcs		5 cm Drop Test					
Test Number	Vertical Stiffness (kN/m)	Shear Stiffness (Nm/°)	Peak Reaction Force (N)	Tyre Maximum Deformation (mm)	Minimum Velocitiy (m/s)	Maximum Velocitiy (m/s)	Minimum Acceleration (m/s²)	Maximum Acceleration (m/s²)
1	128.816	102.608	-2149.500	-1.203	-0.825	0.699	-89.010	120.800
2	128.817	84.085	-2261.800	-1.314	-0.856	0.822	-84.418	70.968
3	134.938	99.594	-2287.150	-1.330	-0.825	0.715	-54.214	83.326
Average:	130.857	95.429	-2232.817	-1.282	-0.835	0.746	-75.881	91.698
Standard Deviation	3.534	9.939	73.259	0.070	0.018	0.067	18.904	25.949
Coefficient of Variation (%)	2.701	10.416	-3.281	-5.429	-2.133	8.980	-24.912	28.299

PNEUMATIC TYRE 4 (P4)	Mechanical Characterisitcs		5 cm Drop Test					
Test Number	Vertical Stiffness (kN/m)	Shear Stiffness (Nm/°)	Peak Reaction Force (N)	Tyre Maximum Deformation (mm)	Minimum Velocitiy (m/s)	Maximum Velocitiy (m/s)	Minimum Acceleration (m/s²)	Maximum Acceleration (m/s²)
1	146.2266548	125.4822777	-2289.300	-0.992	-0.825	0.613	-69.899	69.550
2	153.6135649	132.704244	-2393.830	-1.109	-0.969	0.678	-81.488	120.118
3	152.522792	122.6346044	-2411.030	-1.035	-0.844	0.627	-122.003	73.754
Average:	150.788	126.940	-2364.720	-1.045	-0.880	0.639	-91.130	87.808
Standard Deviation	3.987	5.191	65.879	0.059	0.078	0.034	27.358	28.061
Coefficient of Variation (%)	2.644	4.089	-2.786	-5.620	-8.912	5.338	-30.021	31.957

Appendix 4: Single spoke samples FE visual behaviour

Honeycomb 5mm displacement (Step 1): 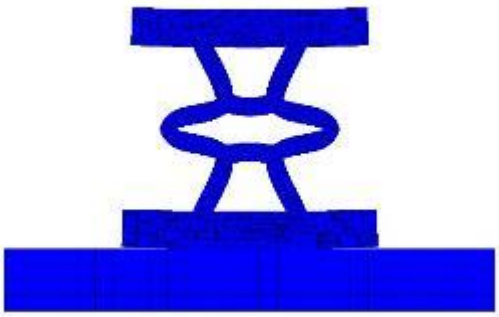	Honeycomb max linear load (Step 2a): 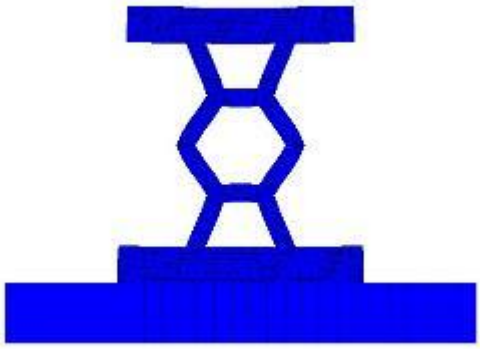
Honeycomb AC rotation +0.5° (Step 2b): 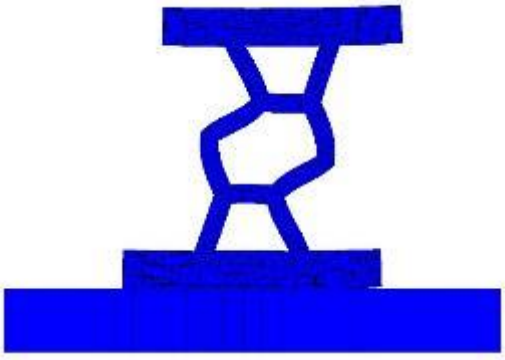	Honeycomb C rotation -0.5° (Step 2c): 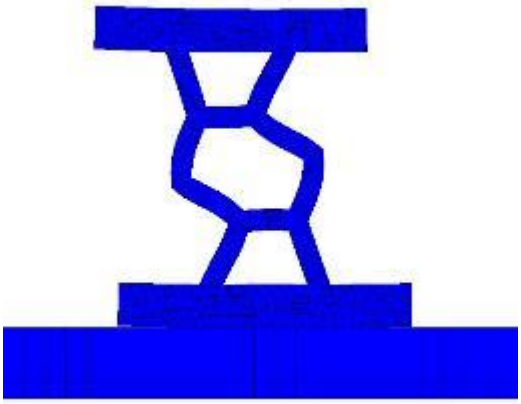
Curved 5mm displacement (Step 1): 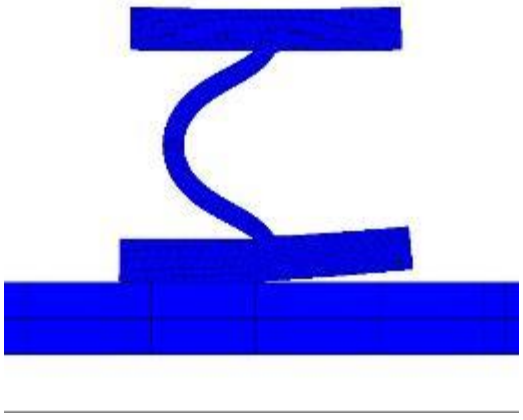	Curved max linear load (Step 2a): 6. 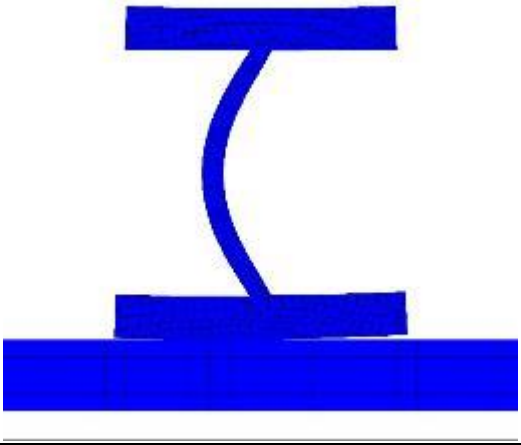

Curved AC rotation +0.5° (Step 2b): 	Curved C rotation -0.5° (Step 2b): 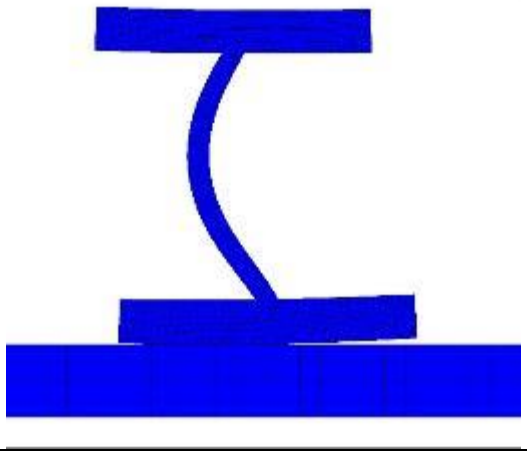
Triangular 5mm displacement (Step 1): 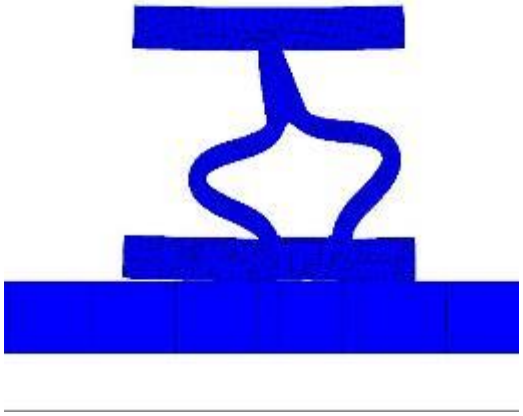	Triangular max linear load (Step 2a): 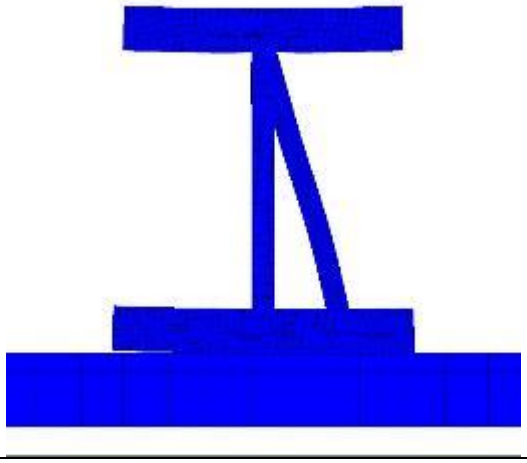
Triangular AC rotation +0.5° (Step 2b): 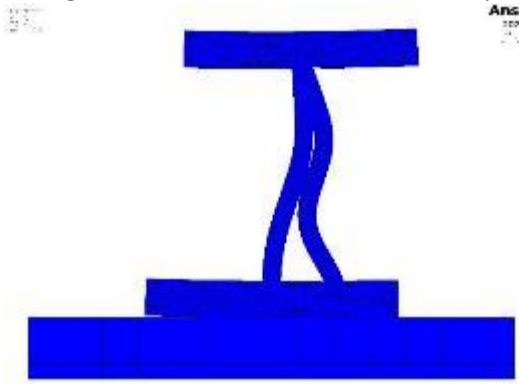	Triangular C rotation -0.5° (Step 2b): 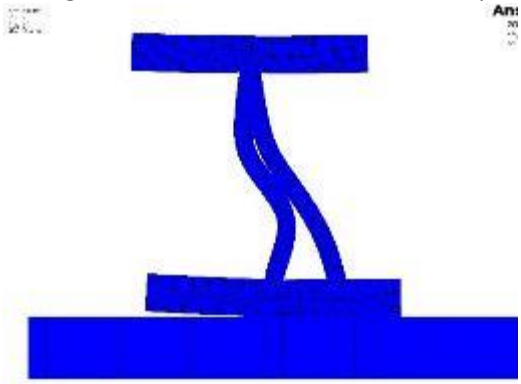

N-spoke 5mm displacement (Step 1): 	N-spoke max linear load (Step 2a): 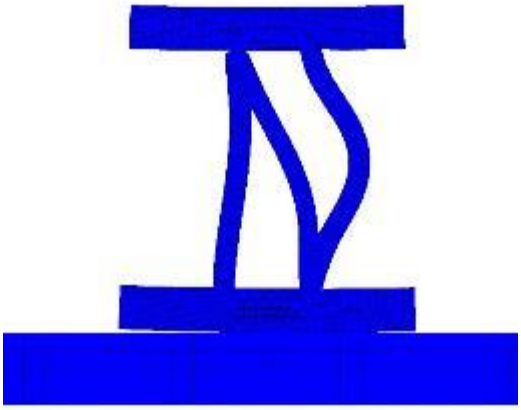
N-spoke AC rotation +0.5° (Step 2b): 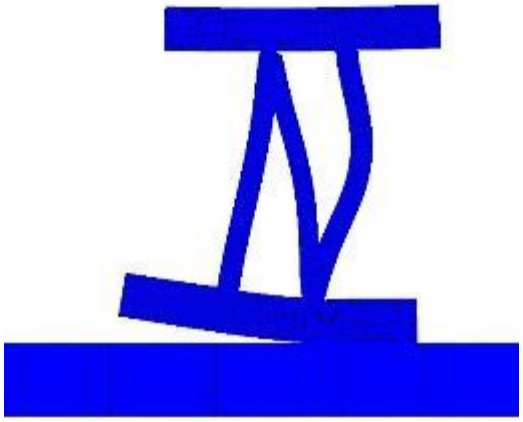	N-spoke C rotation -0.5° (Step 2b):